PIEZOELECTRIC PROPERTIES OF POLYELECTROLYTE MULTILAYER FILMS

A THESIS SUBMITTED TO
THE GRADUATE SCHOOL OF NATURAL AND APPLIED SCIENCES
OF
MIDDLE EAST TECHNICAL UNIVERSITY

BY

ÖZLEM SEVER

IN PARTIAL FULFILLMENT OF THE REQUIREMENTS
FOR
THE DEGREE OF MASTER OF SCIENCE
IN
POLYMER SCIENCE AND TECHNOLOGY

APRIL 2015

Approval of the thesis:

PIEZOELECTRIC PROPERTIES OF POLYELECTROLYTE MULTILAYER FILMS

submitted by **ÖZLEM SEVER** in partial fulfillment of the requirements for the degree of **Master of Science in Polymer Science and Technology Department, Middle East Technical University** by,

Prof. Dr. Gülbin Dural Ünver
Dean, Graduate School of **Natural and Applied Sciences**

Prof. Dr. Necati Özkan
Head of Department, **Polymer Science and Technology**

Prof. Dr. Göknur Bayram
Supervisor, **Chemical Engineering Dept., METU**

Assist. Prof. Dr. İrem Erel Göktepe
Co-Supervisor, **Chemistry Dept., METU**

Examining Committee Members:

Prof. Dr. Necati Özkan
Polymer Science and Technology Dept., METU

Prof. Dr. Göknur Bayram
Chemical Engineering Dept., METU

Assist. Prof. Dr. İrem Erel Göktepe
Chemistry Dept., METU

Prof. Dr. Ahmet Oral
Physics Dept., METU

Assoc. Prof. Dr. Özcan Köysüren
Energy and Materials Engineering Dept., Ankara University

Date: 29.04.2015

I hereby declare that all information in this document has been obtained and presented in accordance with academic rules and ethical conduct. I also declare that, as required by these rules and conduct, I have fully cited and referenced all material and results that are not original to this work.

Name, Last name: ÖZLEM SEVER

Signature:

ABSTRACT

PIEZOELECTRIC PROPERTIES OF POLYELECTROLYTE MULTILAYER FILMS

Sever, Özlem
M.S., Department of Polymer Science and Technology
Supervisor: Prof. Dr. Göknur Bayram
Co-Supervisor: Assist. Prof. Dr. İrem Erel Göktepe

April 2015, 76 pages

Piezoelectric material is the material which converts the electrical energy to the mechanical energy or mechanical energy to the electrical energy. Piezoelectricity is usually considered as a property of ceramic materials because their crystal lattice structure does not have a centre of symmetry, as a result, the unit cells of ceramics contain a small electric dipole. However, after piezoelectric properties of poly(vinylidene fluoride) (PVDF) were discovered, polymeric materials have been preferred over the ceramic ones due to their high flexibility, low cost, high chemical stability, etc.. In order to obtain piezoelectric properties, electrical poling process has to be applied to the materials, which means that they have to be polarized.

Layer-by-layer self-assembly is a technique to produce ultra-thin multilayer films. It is based on alternating deposition of oppositely charged polyelectrolytes at the surface. LbL films have been investigated as potential piezoelectric materials due to polarization within the multilayers, eliminating the electrical poling treatment to obtain a piezoelectric material.

In this study, piezoelectric characteristics of LbL films of different polyelectrolyte pairs, i.e. branched poly(ethylenimine) (BPEI)/poly(styrene sulfonate) (PSS) and poly(diallyldimethylammonium chloride) (PDDA)/PSS have been examined and contrasted. The effect of multilayer thickness on the piezoelectric properties has been specifically examined in detail. Thicknesses of the films were determined using ellipsometer and Atomic Force Microscopy (AFM). AFM analysis was performed also to investigate surface morphology and roughness of the films. In addition, electrical properties such as electrical resistivity of the films were determined with two-point probe method by applying pressure and investigating the change in electrical property. When the applied pressure was increased, volume resistivity values of 41 and 61 layers of BPEI/PSS and PDDA/PSS films decreased, in other words their conductivity increased.

To investigate piezoelectric properties of the films, a multimeter was used to determine voltage change at different pressures. When 2.62 kPa was applied to the film, 5.9 mV and 4.4 mV were obtained from 61 layer BPEI/PSS and PDDA/PSS films, respectively. Piezoelectric properties of the films were also investigated through displacement-electric field hysteresis loop analysis using AFM. Hysteretic behavior of all the films suggested that LbL films had piezoelectric properties. The highest hysteresis amount (%) value for BPEI/PSS film was calculated as 66.8 % for 41 layer film at 30 V voltage application. On the other hand, the highest hysteresis amount (%) value for PDDA/PSS film was found as 84.5 % for 21 layer film at 20 V.

Key Words: piezoelectric property, layer-by-layer films, electrostatic self-assembly technique, displacement-electric field hysteresis loop

ÖZ

ÇOK KATMANLI POLİELEKTROLİT FİLMLERİN PİEZOELEKTRİK ÖZELLİKLERİ

Sever, Özlem
Yüksek Lisans, Polimer Bilimi ve Teknolojisi Bölümü
Tez Yöneticisi: Prof. Dr. Göknur Bayram
Ortak Tez Yöneticisi: Yrd. Doç. Dr. İrem Erel Göktepe

Nisan 2015, 76 sayfa

Piezoelektrik malzeme elektrik enerjisini mekanik enerjiye ya da mekanik enerjisini elektrik enerjisine dönüştürebilen malzemedir. Piezoelektriklik genellikle seramik malzemelerin bir özelliği olarak düşünülmektedir çünkü kristal ağ yapıları merkez simetriye sahip değildir, sonuç olarak seramiklerin birim hücreleri elektriksel iki kutup içermektedir. Fakat poli(viniliden florür)'ün (PVDF) piezoelektrik özellikleri keşfedildikten sonra, polimer malzemeler yüksek esneklik, az maliyet, yüksek kimyasal kararlılıklarından dolayı seramiklerin yerine tercih edilmektedirler. Piezoelektrik özelliklerin elde edilmesi için, malzemeye elektriksel kutuplaşma prosesi uygulanmalıdır. Bunun anlamı da malzemeler kutuplaştırılmalıdır.

Katman-katman kendiliğinden yapılanma çok katmanlı aşırı ince filmleri hazırlamak amaçlı kullanılan bir yöntemdir. Bu yöntem zıt yüklü polielektrolitlerin yüzeyde birbiri ardına kaplanmasına dayanmaktadır. Katman-katman kendiliğinden yapılanan filmler çok katmanlı filmlerin içindeki polarizasyondan dolayı potansiyel piezoelektrik malzemeler olarak incelenmektedir, bu yöntem piezoelektrik malzeme elde etmek için kullanılan elektriksel kutuplaşma işlemini elemektedir.

Bu çalışmada, katman-katman kendiliğinden yapılanan filmlerin piezoelektrik karakteristikleri farklı polielektrolit çiftleri, mesela dallanmış polietilenimin (BPEI)/polistiren sülfonat (PSS) ve polidiallildimetilamonyum klorür (PDDA)/PSS için incelenmektedir ve karşılaştırılmaktadır. Çok katmanlı filmlerin kalınlığının piezoelektrik özellikler üzerindeki etkisi özellikle detaylı olarak incelenmektedir. Filmlerin kalınlıkları Atomik Kuvvet Mikroskobu (AFM) ve ellipsometre kullanılarak belirlenmiştir. Ayrıca filmlerin yüzey yapısını ve pürüzlülüğünü incelemek için de AFM analizi yapılmıştır. Ek olarak, filmlerin elektriksel özdirenç gibi elektriksel özellikleri iki nokta temaslı ölçüm yöntemi ile basınç uygulayıp elektriksel özellik değişimi incelenerek belirlenmiştir. Uygulanan basınç arttırıldığı zaman 41 ve 61 katman BPEI/PSS ve PDDA/PSS filmlerinin hacim özdirenci düşmüştür, diğer bir deyişle iletkenlikleri artmıştır.

Filmlerin piezoelektrik özelliklerini araştırmak için, farklı basınçlarda değişen voltajı belirlemek için bir multimetre kullanılmıştır. Filme 2.62 kPa uygulandığı zaman, 61 katman BPEI/PSS ve PDDA/PSS filmlerinden sırasıyla 5,9 mV ve 4,4 mV elde edilmiştir. Filmlerin piezoelektrik özellikleri, ayrıca yerdeğişim-elektrik alanı histerezis döngü analizi AFM kullanılarak incelenmiştir. Filmlerin histeretik davranışı katman-katman sentezlenen filmlerin piezoelektrik özelliklere sahip olduğunu önermektedir. BPEI/PSS filmi için en fazla histerezis değeri (%), 41 katman filmde 30 V voltaj uygulandığında % 68,8 olarak hesaplanmıştır. Öte yandan, PDDA/PSS filmi için en fazla histerezis değeri (%), 21 katman filmde (20 V) % 84,5 olarak bulunmuştur.

Anahtar Kelimeler: piezoelektrik özellik, katman-katman filmler, elektrostatik kendiliğinden yapılanma yöntemi, yerdeğişim-elektrik alanı histerezis döngü

To my dear family,

ACKNOWLEDGEMENTS

I would like to express my sincere appreciation to my supervisor Prof. Dr. Göknur Bayram for her encouragement and support. First of all, she always guided and helped me during the research and also believed me and my thesis subject all the time. Secondly, she did not avoid anything and we pushed limits together. When the difficulties came up over and over again, she helped and motivated me to understand and solve the problems. It is impossible to think progressing so much without her guidance and support.

I would like to thank my co-supervisor, Assist. Prof. Dr. İrem Erel Göktepe for her guidance and valuable opinions. All the time she helped me and with her guidance I completed my research easily.

I am also very thankful to Prof. Dr. Ahmet Oral and his student Ümit Çelik who is working at Nano-Magnetics Institute for their help. They conducted AFM analysis and helped us to understand hysteresis loop. I would like to thank for AFM analysis, Dr. İbrahim Çam from METU Central Lab.

This study was supported by the Scientific Research Project of METU with the number of BAP-07-02-2014-007-194.

Special thanks to my friends, Esra Bağ, Birsu Kölemen, Duygu Güven, Özlem Çetin, Alyaan Khan and Pelin Yuşan who were always there for me to support and I am very glad to have friends like you. Also thanks to colleagues from chemical engineering department.

If I completed this research, the biggest thank should be given to my fiancée, Ahmet Umur Güngör. Without his love or his existence, it would be much

more difficult to complete my study. He was always thoughtful, patient and full of love. Thank you for being in my life and it is meaningful with you.

Finally, I would like to thank my family. I am really proud of being your daughter and if you did not support and trust me, I couldn’t do anything. This work was not achieved without you, your encouragement and your love. Mom, dad and little sister, I am really glad to be with you.

TABLE OF CONTENTS

CHAPTERS

APPENDICES

LIST OF TABLES

TABLES

LIST OF FIGURES

FIGURES

NOMENCLATURE

A	Cross Sectional Area, m^2
d_{33}	Piezoelectric coefficient, Å/V
$D_{largest}$	Largest difference of displacement at any voltages, nm
D_T	Total displacement change, nm
E	Electric Field, V/nm
I	Electrical Current, Ampere
L	Effective Length of Current Path, cm
R	Electrical Resistance, Ohm
R_s	Sheet Resistance, Ohm/square
T_f	Thickness of film, nm
V	Electrical Voltage, Volt
W	Effective Perimeter of Electrodes, cm

Greek Letters

ρ_v	Volumetric Electrical Resistivity, Ohm.cm
δ	Electrical Conductivity, Siemens/cm

Abbreviations

AFM	Atomic Force Microscopy
BPEI	Branched poly(ethylenimine)
CNT	Carbon Nanotube
DI	Deionized
EAP	Electro-active Polymer
ESA	Electrostatic Self-assembly
LbL	Layer-by-Layer
$LiNbO_3$	Lithium niobate
PDDA	Poly(diallyldimethylammonium chloride)
PSS	Poly(styrene sulfonate)
PVC	Poly(vinyl chloride)
PVDF	Poly(vinylidene fluoride)
P(VDF-TrFE)	Copolymer of vinylidene fluoride (VDF) and trifluoroethylene (TrFE)
PZT	Lead Zirconate Titanate

CHAPTER 1

INTRODUCTION

Dielectric materials can be defined as insulators or very poor conductors of electric current. When electric field is applied to the material, the charges cannot pass through the dielectric; in other words, current does not flow due to the fact that there is no free electron within the material. However, dielectrics can be polarized. Positive and negative charges move with the application of electric field [1, 2].

Dielectrics can be divided into four categories according to their microscopic properties, which are ferroelectricity, piezoelectricity, pyroelectricity and electrostriction. Certain crystalline materials show piezoelectricity which is the ability in order to get electric charge when mechanical stress is applied to the material. After the discovery of piezoelectricity, it was found out that these materials can be used for many useful applications which are generation of high voltages and frequency and the production and detection of sound. They also become the part of daily life. For instance, for lighters, ignition source can be piezoelectric material [1, 3].

The typical single crystalline materials which are quartz, tourmaline and Rochelle salt have disadvantages which are weak piezoelectric effect, low mechanical strength, sensitivity to moisture and narrow operating temperature range. In order to eliminate these disadvantages, polycrystalline ceramic materials took the place of piezoelectric single crystals because piezoelectric ceramics have strong and stable piezoelectric effects and it is easy to produce them into complex shapes and large pieces [3]. Lithium niobate ($LiNbO_3$) and lead zirconate titanate (PZT) can be given as examples for piezoelectric ceramics [1].

Polymers have lots of advantages in an industrial manner when they are compared with the other type of materials. They have light weight and high corrosion resistance, high electrical resistance, high flexibility in structures. Raw material and processes that are used to produce polymers are not expensive. As a piezoelectric polymer, in 1969, properties of poly(vinylidene fluoride) (PVDF) were discovered by Kawai. Moreover, PVDF can be produced into thin films due to its flexibility [4-6].

It is really important to form products for specific application areas. In order to control the supermolecular structures, organic thin film fabrication became a powerful tool for optical elements, surface coatings, biosensor industries, etc. Well-ordered films can be formed with specific properties. If the molecules compete with each other, it is difficult to obtain stable films. On the other hand, if the interaction between molecules is favorable and molecules are perfectly aligned on substrate, then stable and ordered films can be produced [6, 7].

The thin films can be produced autonomously by molecular self-assembly process. In this process, intermolecular interactions such as ionic, hydrogen, van der Waals bonds, etc. are used as driving forces in order to obtain thin films. Nanofabrication steps can be difficult due to the requirements in manipulation of atomic and molecular-levels, however, these difficult nanofabrication steps can be achieved by self-assembly process. Contacts between complementary units such as anionic and cationic molecular segments reject impurities and incorrect units. These polyanions and polycations are adsorbed alternately by dipping into aqueous polyelectrolyte solutions. This process is called as electrostatic self-assembly (ESA) process. The other name of the process is layer-by-layer (LbL) self-assembly technique. Using ESA process, composition of each layer can be easily controllable and also deposition parameters can change the structure of each layer [7].

The main purpose of this study was to investigate piezoelectric properties of polyelectrolyte multilayer films which were deposited onto the substrate through layer-by-layer technique. Branched poly(ethylenimine) (BPEI) and poly(styrene sulfonate) (PSS) were chosen as polycation and polyanion for the first system, respectively. In addition, poly(diallyldimethylammonium chloride) (PDDA) and PSS were selected as polycation and polyanion for the second system, respectively. Indium tin oxide (ITO) coated glass, silicon wafer slide and quartz slide were used as substrates. Synthesized films were examined in terms of their piezoelectric characteristics. Variation of number of layers was one of the parameters of the system. 1, 2, 3, 21, 41 and 61 layers of BPEI/PSS and PDDA/PSS were deposited onto the substrates. LbL growth of thin films and their thicknesses were determined by ellipsometry. Furthermore, surface topography and roughness values of films were displayed by Atomic Force Microscopy (AFM). In order to confirm, thickness of films was also specified by AFM. To characterize electrical property of the films, electrical resistivity measurements were conducted by two-point probe method. Resistivity changes were obtained with the application of pressure. Moreover, piezoelectric properties of films were characterized through voltage output measurement and hysteresis loop analysis. Multimeter was used to determine voltage output at different pressures. Displacement-electric field hysteresis loop was conducted by AFM again.

CHAPTER 2

BACKGROUND

2.1 Piezoelectricity

2.1.1 Piezoelectric Characteristics

In wide range applications, piezoelectric materials which can be used as sensors and actuators have been chosen due to their electro-mechanical characteristics [8]. Piezoelectric materials have two basic characteristics which are direct and converse piezoelectric effects. In direct piezoelectric effect, electrical charge or voltage can be obtained when mechanical force or pressure is applied to the piezoelectric material. Moreover, when electrical charge or voltage is given to the material, mechanical force or strain can be generated. This is called as converse piezoelectric effect. These characteristics provide usage of piezoelectric materials as sensors and actuators [9, 10].

2.1.2 History of Piezoelectricity

Pierre and Jacques Curie discovered direct piezoelectricity or pressure electricity in 1880. The combination of knowledge about pyroelectricity and structure of crystallinity assisted to discover this phenomenon. Furthermore, in 1881, Lippmann found out the converse piezoelectric effect. The name of the piezoelectricity came from the Greek word piezein which means to squeeze or press. It was firstly used as transducers during World War I [3, 11]. After World War II and exploration of PZT, numerous applications were developed. One of them was energy harvesting. Generation of electricity from ambient motion and vibration is the essential goal when power sources cannot be available or usable. Energy harvesting provided new doors and opportunities for applications and novelties. PZT has the maximum piezoelectric response as it is compared with the other piezoelectric ceramics [3].

After the discovery of properties of PVDF by Kawai, different electro-active polymers (EAPs) such as nylon, polyvinyl chloride (PVC), etc. were studied in order to understand whether they show piezoelectricity or not [8, 12]. Polypropylene, polystyrene, poly(methyl methacrylate), vinyl acetate and odd number nylons have piezoelectric properties but they do not show piezoelectric effect as strong as PVDF and copolymer of vinylidene fluoride (VDF) and trifluoroethylene (TrFE) (P(VDF-TrFE)) do [13].

2.1.3 Principles of Piezoelectricity

Changes in the internal polarization which means simply separation of positive and negative charges are the main idea of the piezoelectricity. There are two polarization mechanisms of dielectric materials, especially piezoelectric polymers. These mechanisms are dipolar and interfacial polarization. Dipolar polarization can be observed when electric field is applied to the material. In this polarization, dipoles rotate and align parallel to the applied electric field. Thus, polarization can be provided with applying sufficient electric field and this is called as poling treatment [8, 14]. The degree of polarization is related with the piezoelectricity of the materials. When the applied electric field is increased, piezoelectric properties also increase. The dielectric breakdown of the material limits the needed value of electric field for poling. For piezoelectric polymers, it is difficult to perform high electric fields to materials due to texture, surface impurities, cracking and etc. Furthermore, interfacial polarization can be provided with electrically heterogeneous materials, i.e. carbon nanotubes (CNTs)-PVDF. Mobile charges within the CNTs can enhance polarization of the material [8].

2.1.4 Piezoelectric Polymers

PVDF and and its copolymer P(VDF-TrFE) are piezoelectric polymers. PVDF has four crystalline phases which are α, β, δ and γ. The most common and stable one is the α-phase and it is non-polar [15]. Additionally, β crystalline phase is the polar one which forms dipole between the fluorine and hydrogen atoms [8]. Chemical structure of PVDF can be seen in Figure 2.1. In α-phase, there is no net surface charge due to random orientation of the dipoles. The dipoles cancel out each other. However, dipoles are oriented when poling treatment is applied to PVDF which shows α-phase. The dipoles become parallel to each other due to charge separation in β-phase. Furthermore, this phase is really important due to the fact that dipole moment of β-phase is very high. In order to obtain piezoelectric property of PVDF, β-phase formation is needed [16].

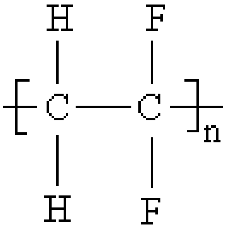

Figure 2.1 Chemical structure of PVDF.

Normally, PVDF shows α-phase. As it was mentioned, to get β-phase, poling treatment can be applied to the material. Nonetheless, when PVDF is mechanically stretched, β-phase can also be obtained. Additionally, P(VDF-TrFE) has β-phase by itself. Therefore, for P(VDF-TrFE), there is no need to do poling treatment or stretching mechanically [8, 16]. Huge electronegativity difference between fluorine, carbon and hydrogen atoms forms its properties. P(VDF-TrFE) has the same phase configuration like PVDF. It has also α, β, δ and γ phases [17].

2.1.5 Application Areas of Piezoelectric Materials

As it was mentioned, piezoelectric materials can be used as sensors. To monitor the cable tension of cable-stayed bridges, for example PVDF film is chosen. With frequency analysis, cable tension is measured [18]. Also, to monitor health and diagnose the damage and its severity, PVDF film is selected as sensing element. Vibration amplitude of the damaged structure is observed [19]. PVDF shock sensors are studied in order to understand piezoelectric response of PVDF under high-pressure shock compression. Up to 25 GPa, PVDF gives reproducible data [20].

Piezoelectric material can also be a transducer for smart materials. Generation and detection of Lamb waves in plates can be developed with PVDF transducers [21]. When P(VDF-TrFE) is used as transducer, it can generate ultrasonic pulse. Polymer transducer also acts as actuator in the system and sends sound wave to the line [22]. An adaptive mirror system is made by PVDF film and laminar glass plate. PVDF piezoelectric film is fixed tightly on one of the surfaces of glass plate and the other surface is evaporated with silver. The mirror part of the system is the evaporated surface. When the voltage is applied to PVDF, deformation of mirror occurs smoothly [23].

Energy harvesting from ambient mechanical sources gives opportunity to design self-powered electronic devices. Nanogenerators are improved to produce self-sufficient power. The main unit of the nanogenerators is piezoelectric nanowires. PVDF nanofibers are used for harvesting mechanical energy from high frequency acoustic waves and low-frequency vibrations/frictions [24]. Wearable microelectronics are the another application area of piezoelectric materials. It is possible to alter batteries with the energy harvesters. For instance, shoe-mounted piezoelectric materials can scavenge electricity during walking. PZT and PVDF stave are used in this system to capture energy of heel-strike and harness energy of sole-bending, respectively

[25]. Also, energy harvesting from backpack can be accomplished by different forces between the wearer and the pack. Traditional backpack shoulder straps are changed with the piezoelectric PVDF [26].

There are some lesser-known applications of piezoelectric polymers. PVDF is a good candidate for a touch or tactile sensor because of its low weight, good mechanical properties and producibility into thin sheets. In order to diagnose and treat various foot disorders and monitor skin condition, tactile sensors are improved. An active palpation sensor is made to determine prostate cancer and hypertrophy. This sensor comprises of PVDF which is placed on the sponge rubber. Furthermore, piezoelectric polymers can be used as energy converters in oceans and rivers. The structure of these converters is named as Energy Harvesting Eel. The test is conducted in a flow tank with PVDF prototype [27].

Piezoelectric polymers were also used in a spacecraft named Stardust which was launched on 7 February 1999 and attained with the comet 81P/Wild 2 on 2 January 2004. Spacecraft consists of Dust Flux Monitor Instrument (DFMI) which contains two PVDF sensors. Particle flux variations, mass distribution in the coma of the comet can be observed, and dust measurements can be done by the instrument. PVDF sensors are placed into DFMI to detect particles of masses in the range of 10^{-11} and 10^{-4} g. When dust particle strikes to PVDF sensors, electrical pulses are generated and this leads to understand the distance between the spacecraft and the comet [27].

2.2 Thin Film Fabrication

Synthesis of conventional piezoelectric and EAP films can be accomplished by spin coating, casting and sol-gel technology. However, using these processes, formation of ultrathin film is difficult. In order to develop and design multifunctional, ultra-small devices, synthesis process has to allow active-thin film formation at the molecular level and also the internal structure of the material has to be controlled. Electrostatic self-assembly (ESA) process can be used for the formation of ultrathin piezoelectric films without poling treatment because of spontaneous polarization, and this technique can provide desired properties and processing route [28, 29]. Furthermore, not only electrostatic interaction but also hydrogen bonding, charge transfer interaction, molecular recognition and coordination interactions can drive the formation of multilayer thin films. Polyelectrolytes, colloid and nanoparticles, dyes, dendrimers, clay minerals, carbon materials, enzymes and proteins, DNA, viruses can all be used as building blocks for LbL self-assembly. These multilayers can be used as chemical and biochemical sensors, optical switches and filters, light emitters, conductive films, ferroelectric and piezoelectric devices, electro-optics and non-linear optics [30-32].

2.2.1 Electrostatic Self-assembly (ESA) Process

The main principle of the ESA process is the interaction between polyanions and polycations. Negatively charged substrate is immersed into the polycation solution. The polycation chains are deposited at the surface via electrostatic interactions resulting in formation of a monolayer. Molecular order of individual monolayers is almost excellent because electrical charge distribution on the surface is uniform. After the removal of the substrate from positive solution, it is rinsed with water or buffer solution. Rinsing procedure is necessary in order to get rid of the loosely bounded polymers. Secondly, the substrate is dipped into polyanion solution and the same procedure can be followed until the desired number of layers is deposited at the surface [7]. Schematic of LbL self-assembly technique based on alternating deposition of positively and negatively charged species at the surface is illustrated in Figure 2.2.

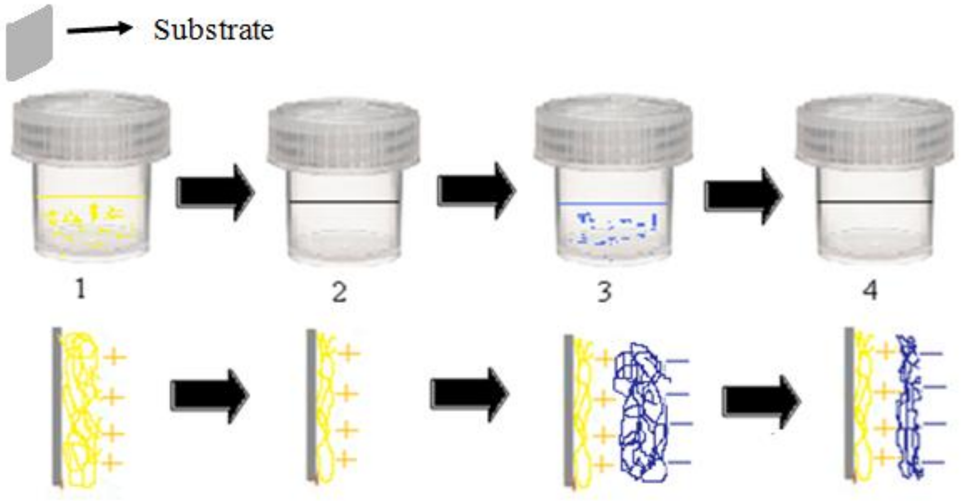

Substrate and assembly of first polyelectrolyte monolayer

Assembly of second polyelectrolyte monolayer

Figure 2.2 Schematic of LbL technique based on alternating deposition of positively and negatively charged species at the surface (1: Polycation solution, 3: Polyanion solution, 2, 4: Rinsing solutions).

Properties of LbL films are primarily affected by the nature of the polymers. For example, it is possible to alter charge density of weak polyelectrolytes by changing pH. Such changes in pH result in conformational changes in the polymer chains and affect the thickness of the multilayer films. In contrast, strong polyelectrolytes are fully charged in solution at a wide range of pH [30, 33]. Therefore, multilayers of strong polyelectrolytes do not show pH-response.

Electrical properties of the films can be altered using hydrophilic weak polyelectrolytes, because ion mobility is affected by hydrophilicity of the LbL film. Water which is absorbed in hydrophilic films facilitates the ion transport. Absorption of water causes increase in ionic conductivity. For example, in order to enhance ion transport, hydrophilic weak polyelectrolytes can be used at or near their pK_a values, which cause decrease in ionic cross-linking (charge density). This decrease leads to looser film structure than that of highly ionic crosslinked multilayers resulting in absorption of higher amount of water. On the contrary, highly ionically cross-linked films are not good ion-exchanger. For instance, when the negatively charged poly(styrene sulfonate) (PSS) and positively charged poly(diallyldimethylammonium chloride) (PDDA) are deposited onto a substrate through LbL self-assembly technique, the resulting film is highly ionically cross-linked and the ion transport of the film is insufficient [34]. In order to control ionic crosslink density, salt can be added to the assembly solutions. When salt is used, charges on the polymers can be partially screened leading to a change in the conformation of the polyelectrolyte from extended to more coiled conformation. In this way, thicker and looser films can be obtained and the amount of water absorbed within the multilayers can be increased [35].

2.2.2 Advantages of ESA process

There are lots of advantages for ESA process when it is compared with traditional methods such as spin coating, sol-gel technology, etc. [28]. ESA process provides excellent nano-scale control in film thickness. The process does not require a chemical reaction and covalent bond formation [7]. Perfect molecular order limits the defects so absence of defects gives long-term environmental robustness to the films. It is possible to coat polymers onto nearly any solid substrates at room temperature and atmospheric pressure. The main advantage of the process is ease in production and it does not require expensive equipments. As it is mentioned before, ESA process occurs through alternating deposition of anionic and cationic polymers at the surface. Optical, electronic, thermal and mechanical properties of the films can be controlled by choosing the appropriate polymer pairs as building blocks or incorporating functional molecules within the multilayers. Moreover, the LbL process is eco-friendly. While producing the films, power is not needed, volatile organic compounds are not used and polymers are dissolved in water or buffer solutions. Substrates with any size or shape can be used to construct multilayers [7].

2.3 Characterization Methods

2.3.1 Thickness Measurement

Growth of LbL films was followed by measuring the thickness of the dry films using an ellipsometer. Ellipsometry is based on sending a linearly polarized light beam to the surface of the sample, which is then reflected to detector. Using this technique, it is possible to get information about thickness of each layer [36].

2.3.2 Electrical Resistivity/Conductivity Measurement

Electrical conductivity value can be calculated from measured resistance value of a material. The relation between electrical resistivity, conductivity and resistance can be seen in Equation 1 [37].

$$R = \rho_v \text{ x } (L/ A_{cs}) = (1/\delta) \text{ x } (L/A_{cs}) \qquad (1)$$

Resistance is represented as R (Ω), volume resistivity and conductivity are shown in this equation as ρ_v (Ω.cm) and δ (S/cm), respectively. Length of current path is L (cm) and cross-sectional area of current path is A_{cs} (cm^2) [37]. Schematic of dimensions of volume resistivity is demonstrated in Figure 2.3.

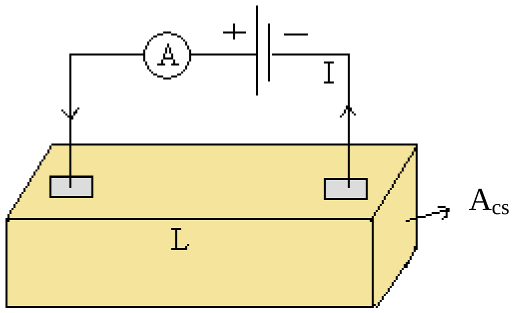

Figure 2.3 Schematic of dimensions of volume resistivity.

There is also a sheet resistance (surface resistivity) definition which is electrical resistance of the surface. Sheet resistance (surface resistivity) formula can be seen in Equation 2. R_s is the sheet resistance (Ω/sq), W is the effective perimeter of electrodes (cm) [38, 39].

$$R_s = R \times (W/L) \qquad (2)$$

Electrical resistivity value can be obtained using two-point probe method, three-point probe method and four-point probe method. As it is understood from the methods' name, number of probes is important. Figure 2.3 also shows schematic illustration of the two-point probe method. Principle of the method is that current passes through the probes in order to measure the resistance of the sample. Ammeter which is represented as A measures the electric current (I) [40].

The difference between two-point probe and four-point probe methods is that four-point probe method eliminates contact resistance and it is independent from contact shape and size [41]. In this study, electrical resistivity values were obtained by two-point probe method. Resistivity changes at various pressures were investigated. Contact resistance was minimized using silver paste.

2.3.3 Voltage Output Measurement

Piezoelectric properties of the multilayer films can be investigated through voltage output measurement. In our study, multimeter was used to specify voltage output at different pressures thorough putting different weights onto LbL film. In this measurement, weight was used as one electrode and ITO/glass was used as another one, which can be seen in Figure 2.4.

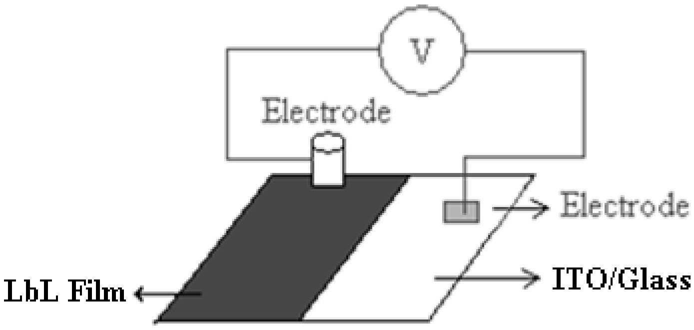

Figure 2.4 Schematic of mechanism of experiments.

2.3.4 Atomic Force Microscopy (AFM) Analysis

AFM can be used to obtain information about surface roughness and morphology of a sample [42]. Moreover, film thickness measurements can also be performed using AFM. An AFM device is composed of a tip, cantilever, chip, focused laser beam and quad photodiode. Flexible microcantilever which is attached to a chip is bended under impression of force, and there is a sharp tip at the end of the cantilever. It is attached to a spring. Compression and extension of spring cause bending of cantilever upward and downward. So, tip is contacted with a sample surface and moved through the surface. Additionally, laser beam is reflected to photodiode and bending is measured. Besides, morphological information about the sample, topography of a surface can also be determined by AFM in three-dimensional (3D) detail. 2D array can be obtained over the surface at each point [42].

AFM can also be performed for determination of hysteresis behavior of piezoelectric materials. Hysteresis loop is used to investigate the behavior of a piezoelectric device under voltages or electric field. In all piezoelectric materials, hysteresis behavior always exists. Hysteresis behavior can be shown as displacement-voltage or displacement-electric field hysteresis loop. When voltage is applied to a material, change in polarization causes extension and retraction of the material and displacement changes are recorded. Then, amount of hysteresis in a material can be calculated by dividing largest difference of displacement for any voltages with total displacement [3]. Additionally, there is a term called as maximum strain (%) which is the ratio of maximum displacement change to the thickness of the material [43]. Furthermore, d_{33} which is a piezoelectric coefficient can be calculated from the slope of linear portion of hysteresis loop by dividing the displacement change (ΔD) with the voltage change (ΔV) [44].

2.4 Previous Work

2.4.1 Piezoelectric Thin Films Synthesized by ESA Process

Zeng and coworkers [28] synthesized piezoelectric films by ESA process. They used PDDA and PSS as oppositely charged polymer pairs for piezoelectric LbL film preparation. Single crystal silicon, quartz, and indium tin oxide (ITO) coated glass were used as substrates. The piezoelectric response of the thin films was determined as follows: Force was applied to the system by dropping the weight onto the film, which was similar to mechanism demonstrated in Figure 2.4. Change in electrical energy was recorded for 50 bilayer PDDA/PSS film (65 nm, measured by ellipsometry). ITO/glass was used as one electrode, and contact area of the weight which was made contact with the multilayer self-assembled film was used as the other electrode. They observed that when applied force was increased, output voltage of self-assembled PDDA/PSS film also increased. The relationship between force and voltage was approximately linear. Therefore, Zeng and coworkers claimed that PDDA/PSS ultrathin film which was synthesized by ESA process had piezoelectric characteristics. Then, d_{33} was calculated as 6.0 pC/N. This result showed that without poling treatment, piezoelectric ultrathin films can be synthesized through LbL technique [28].

In another study, Zeng and coworkers [29] synthesized piezoelectric thin films from PDDA and poly-S-119 comprised of poly(vinylamine) backbone with an anionic azo chromophore. First, platinum (Pt) nanoclusters were mixed with PDDA, so Pt:PDDA clusters which provided positive charges were formed. Poly-S-119 was used as an anionic polyelectrolyte. Then, Pt:PDDA/poly-S-119 was deposited onto the substrates which were the single crystal silicon and aluminum-coated conductive flexible polymer film. In this study, polymer (poly-S-119)/platinum nanocluster (Pt:PDDA) composite film fabrication through LbL technique was investigated [7, 29]. In experiments, the top part of the film was fixed, and glass was used for this purpose. Moreover, the bottom part was kept free. To understand piezoelectric response of the film, small dc voltage which was maximum 12 V was applied to the 11 bilayer LbL film (30.2 nm, measured by ellipsometry) and film displacement was measured. They obtained the hysteresis loop directly by the measurement of polarization of film when external voltage was applied. Zeng and coworkers [29] indicated that hysteretic behavior of multilayer thin film under electric field proved that piezoelectric thin film could be synthesized by ESA process without poling treatment. Also they suggested that the net macroscopic polarization could be achieved by ESA process [29, 45].

2.5 Motivation of the Study

ESA process and piezoelectric polymers individually provide wide range of application areas. On the other hand, combination of piezoelectric polymers and ESA process is new. In the literature, the number of studies on piezoelectric LbL films is limited. There are only 2 papers and a patent about piezoelectric polymer films which have been prepared via ESA [28, 29, 45]. In all these studies, PDDA was used as the cationic polyelectrolyte during the preparation of the films. Piezoelectric properties of different polymer pairs and the effect of multilayer thickness on the piezoelectricity of the films have not been examined before in detail. This has been the primary motivation of the work. In this study, it has been aimed to study piezoelectric properties of two different LbL films, composed of BPEI/PSS and PDDA/PSS polymer pairs. The multilayers were characterized in terms of thickness, surface morphology, electrical properties, and piezoelectric properties which are voltage output and displacement-electric field hysteresis loop. The effect of number of layers on the piezoelectric properties of the thin films has also been investigated.

CHAPTER 3

EXPERIMENTAL

3.1 Materials

Branched poly(ethylenimine) (BPEI; M_w = 25,000 g/mole), poly(sodium 4-styrenesulfonate) (PSS; 30 wt% in H_2O, M_w = 70,000 g/mole) and poly(diallyldimethylammonium chloride) (PDDA; 20 wt% in H_2O, M_w = 100,000-200,000 g/mole) were purchased from Sigma-Aldrich Co. Sodium dihydrogen phosphate dihydrate ($NaH_2PO_4{\cdot}2H_2O$; M = 156.02 g/mole) was purchased from Merck Chemicals. Indium tin oxide (ITO) coated glass slides, quartz slides and silicon wafers were used as substrates. Surface resistivity of ITO/glass is 15-25 Ω/sq [46]. Isopropyl alcohol (99.8 wt%) was purchased from Aklar Kimya. Table 3.1 demonstrates chemical structures of the polymers.

Table 3.1 Chemical structures of the polymers used.

Name	Chemical Structure
Branched poly(ethylenimine) (BPEI)	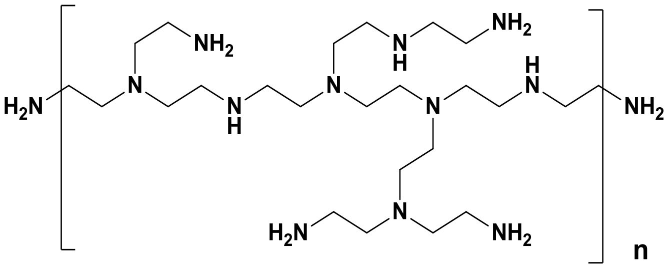
poly(sodium 4-styrenesulfonate) (PSS)	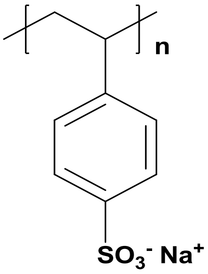
poly(diallyldimethyl ammonium chloride) (PDDA)	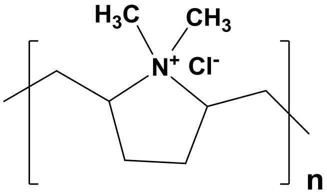

3.2 Experimental Procedure

3.2.1 ESA Process

3.2.1.1 Cleaning Procedure

ITO/glass substrates were cut into 1.5 x 2.5 cm^2 pieces and then first immersed into deionized (DI) water for 15 minutes in ultrasonic bath. A few drops of dishwashing liquids were added into DI water as well. Then, the substrates were rinsed consecutively with tap water, distilled and DI water. Nitrogen gas flow was used to dry the substrates. Secondly, the substrates were treated with acetone for 15 minutes in the ultrasonic bath. The reason of treatment with DI water and acetone is to remove impurities from the surface. After acetone treatment, the substrates were again rinsed and dried under N_2 flow. Lastly, the substrates were treated with isopropyl alcohol for 15 minutes in the ultrasonic bath. The same rinsing and drying procedure was followed.

Silicon wafers and quartz slides were cleaned using the following procedure. First, the substrates were treated with concentrated sulfuric acid for 1 hour and 25 minutes. Then, the substrates were rinsed with DI water and dried under N_2 flow. Second, the substrates were immersed into 0.25 M NaOH solution for 10 minutes followed by rinsing and drying steps.

3.2.1.2 Multilayer deposition

BPEI, PSS and PDDA were separately dissolved in 0.01 M phosphate buffer at pH 5. Concentrations of polymer solutions were 0.5 mg/mL. After the cleaning procedure, 1 layer of BPEI was coated onto the substrate as a precursor layer for 1 hour. Then, the substrate was dipped into PSS solution for 10 minutes in order to obtain the second layer. Two rinsing steps were performed between the polymer deposition steps. 0.01 M phosphate buffer at pH 5 was used as the rinsing solution. Then, the substrate was alternatingly immersed into BPEI and PSS solution for 10 minutes each, until desired number of layers was achieved. All substrates were immersed into solutions vertically. For PDDA/PSS system, the same film preparation procedure was used. 2, 21, 41 and 61 layers of BPEI/PSS and PDDA/PSS films were prepared. Schematic of deposition of polyelectrolyte layers at the surface can be seen in Figure 3.1.

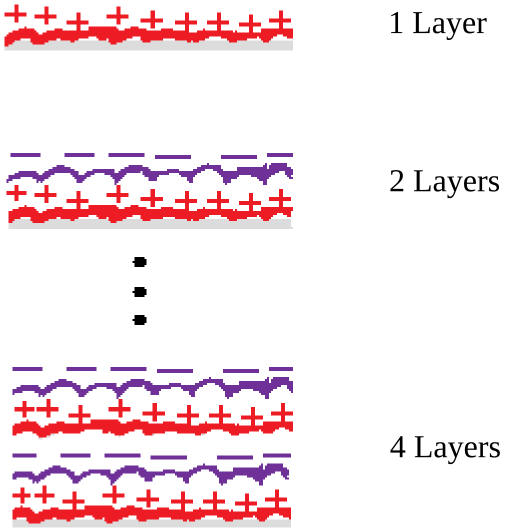

Figure 3.1 Schematic of deposition of polyelectrolyte layers at the surface.

3.3 Characterization Methods

All measurements were conducted at room temperature. 1 g, 2 g, 3 g and 5 g of weights were put onto the silver disc (radius = 0.25 cm) which was put onto LbL film and measurements were performed in terms of electrical resistivity and voltage output values. The purpose of using silver disc was to provide equal distribution of the applied pressure. Then, amount of weights was converted to pressure using gravitational constant and area of the silver disc (0.2 cm^2). 1 g, 2 g, 3 g and 5 g were found as 0.62 kPa, 1.12 kPa, 1.62 kPa and 2.62 kPa, respectively.

3.3.1 Ellipsometry

Film thickness was recorded using a Spectroscopic Ellipsometer of Optosense, USA (OPT-S6000). Reported data obtained from ellipsometry were the average of 4 different measurements which were taken from different locations on the coated silicon wafer. Figure 3.2 shows the ellipsometer used in this study.

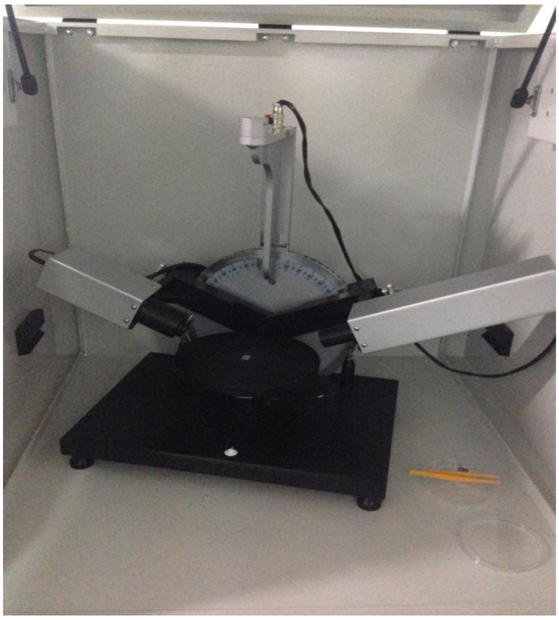

Figure 3.2 Photograph of ellipsometer.

3.3.2 Two-point Probe Method

Electrical resistivity/conductivity measurements were conducted using a two-point probe method. A Keithley 2400 Resistivity Tester which can be seen in Figure 3.3 was used for this purpose. After deposition of polyelectrolytes onto substrates, silver paste was coated with 0.4 x 0.4 cm^2 sized squares onto both LbL synthesized film and ITO/glass in order to minimize contact resistance. Copper wires were attached to silver paste as it can be seen in Figure 3.4. Crocodile clamps were hooked to the wired electrodes during the measurements. Voltage of 2 V was kept constant in resistivity tester. Moreover, when pressure was applied to LbL film, weights were used as an electrode, and resistance values of the LbL films were recorded. Then, volume resistivity was calculated from Equation 1. Reported volume resistivity values are the average of at least 10 measurements.

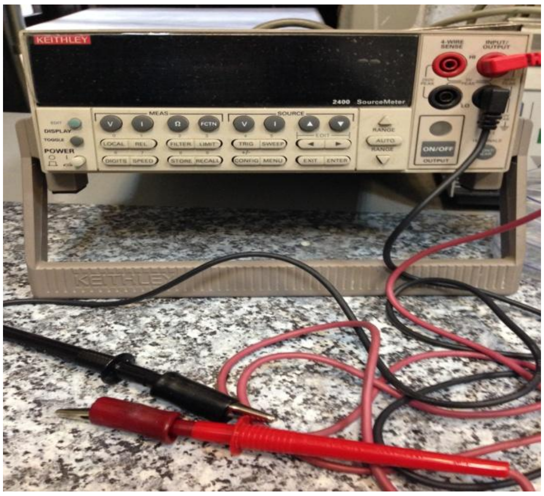

Figure 3.3 Photograph of Keithley 2400 Resistivity Tester.

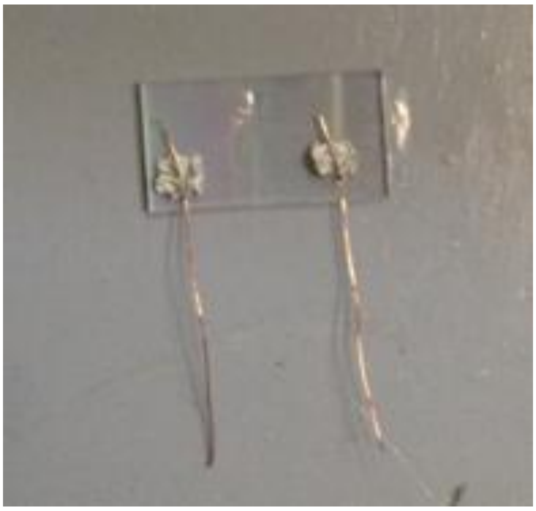

Figure 3.4 Representation of wired electrodes attached with silver paste.

3.3.3 Voltage Output Measurement

Piezoelectric properties of films were determined through a TTT-ECHNI-C VC97 digital multimeter which was illustrated in Figure 3.5. Direct current (DC) was applied to the films, and voltage output was recorded when pressure was applied to thin films. Weights were used as one electrode and ITO/glass was used as another electrode. Moreover, pressure was applied using crocodile clamps only which were attached to multilayer thin film and ITO/glass, and voltage was recorded. The main idea behind this was to take the crocodile measurement without weight as a reference point and understand progress of voltage output values clearly. Reported voltage output data were the average of at least 5 measurements.

Figure 3.5 Demonstration of digital multimeter.

3.3.4 AFM Analysis

Morphological analysis of the 42 layers of BPEI/PSS and PDDA/PSS films which were deposited onto silicon wafers were performed using a Veeco MultiMode V instrument in dynamic mode at the Central Laboratory, METU. Furthermore, displacement-electric field hysteresis loop and surface morphology analysis were conducted by Ambient AFM/MFM in tapping and dynamic mode at Nano-Magnetics Instruments. For this purpose, 1, 2, 3, 21, 41 and 61 layers of BPEI/PSS and PDDA/PSS were deposited onto ITO/glass and were investigated in order to determine whether they show hysteretic behavior or not. Average roughness (R_a) values were recorded. Equation of R_a is given in Equation 3. Distance from the mean line is represented as y_i for the i^th^ data [47].

$$R_a = (1/n) \times \sum_{i=1}^{n} \left| y_i \right| \qquad (3)$$

CHAPTER 4

RESULTS AND DISCUSSION

In this study, main goal is to synthesize piezoelectric polymer films by ESA process. First, two different electrostatic polyelectrolyte multilayers, i.e. BPEI/PSS and PDDA/PSS films were prepared using LbL technique. Thickness of the films was determined by both ellipsometry and AFM. Surface morphology analysis was performed by AFM. To characterize electrical resistivity/conductivity properties, a two-point probe method was used. Changes in electrical resistivity were determined by applying different pressures. To investigate piezoelectric properties, voltage output measurement and displacement-electric field hysteresis loop analysis were conducted. Voltage output was measured at various pressures. Lastly, hysteresis loop analysis was conducted by AFM. Results of two different film systems (BPEI/PSS and PDDA/PSS films) were compared to understand the effect of film structure on the piezoelectric properties of the films.

4.1 Multilayer Characterization

4.1.1 LbL Growth of Thin Films

Ellipsometry was used to follow LbL growth of BPEI/PSS and PDDA/PSS multilayers at pH 5. The changes in film thicknesses with increasing number of layers or bilayers for BPEI/PSS and PDDA/PSS are reported in Figures 4.1 and 4.2, respectively.

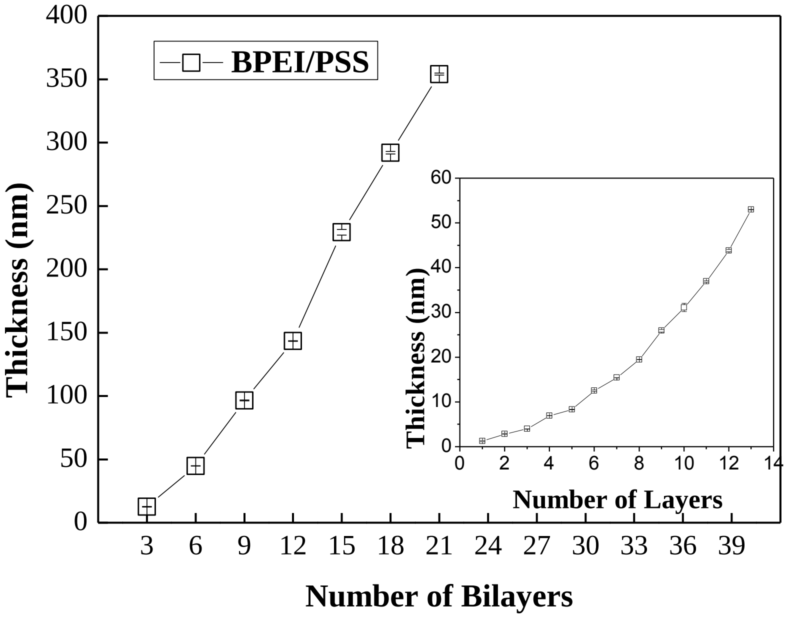

Figure 4.1 Thickness of BPEI/PSS film as a function of bilayer number at pH 5.

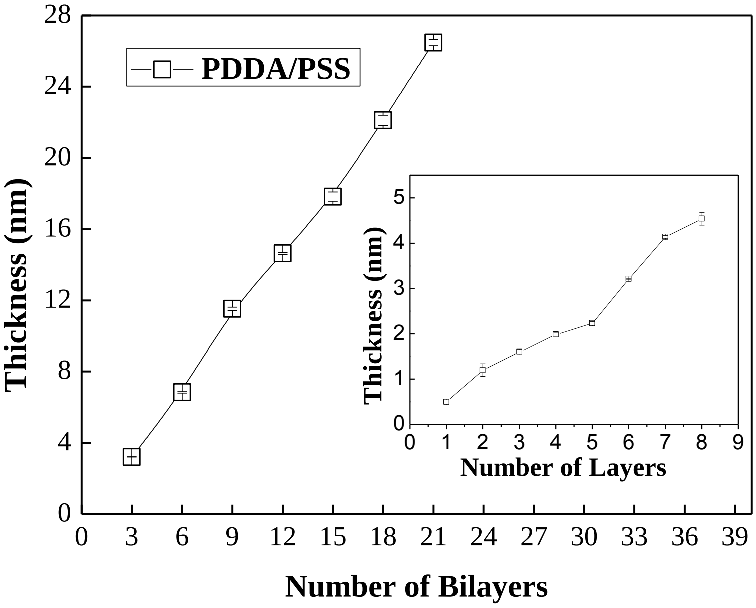

Figure 4.2 Thickness of PDDA/PSS film as a function of bilayer number at pH 5.

As it is seen in the figures, when number of layers is increased, thickness of the films also increases, indicating successful growth of the LbL films. The growth profile for PDDA/PSS film is linear (Correlation coefficient, R^2 = 0.999 for linear fit). PDDA and PSS are both strong polyelectrolytes which associate with each other through many binding points resulting in intense and very thin films [34, 48]. On the other hand, the growth profile for BPEI/PSS pairs was found to be exponential (R^2 = 0.997 for exponential fit). Note that the correlation coefficient for an exponential growth became higher than that for a linear growth as the number of layers is increased for BPEI/PSS films. The difference in the growth profiles of BPEI/PSS and PDDA/PSS multilayers may be correlated with the difference in surface roughness of the films. The charge density on BPEI and PDDA chains is different at pH 5. BPEI is a weak polyelectrolyte (pK_a = 8.2-8.3) and has lower charge density than PDDA (a strong polyelectrolyte) at pH 5. Therefore, the number of binding points between BPEI and PSS layers is lower than that between PDDA and PSS layers, resulting in thicker films with loopy structure and higher surface roughness for BPEI/PSS films. Higher surface roughness increases the surface area and leads to deposition of higher amount of material at the surface which may lead to exponential growth of the film [49-51].

To study piezoelectric properties, 2, 21, 41 and 61 layers of BPEI/PSS and PDDA/PSS were deposited at the surface. Thickness values obtained by ellipsometry are tabulated in Table 4.1. As it was mentioned before, AFM was also used to determine thickness of the films. Table 4.2 contrasts thickness values of 42 layers of BPEI/PSS and PDDA/PSS films which were obtained from ellipsometry and AFM. Thickness values obtained by AFM were the average of 10 measurements, which can be seen in Appendix A.

Table 4.1 Ellipsometric thickness of BPEI/PSS and PDDA/PSS films for different number of layers.

Number of Layers	Average Thickness (nm) of BPEI/PSS films	Average Thickness (nm) of PDDA/PSS films
2	2.89 ± 0.07	1.20 ± 0.14
21	132.71 ± 1.56	13.22 ± 0.01
41	325.90 ± 4.26	26.14 ± 0.29
61	856.41 ± 1.24	46.24 ± 0.46

Table 4.2 Thickness values obtained from ellipsometry and AFM for 42 layers of BPEI/PSS and PDDA/PSS.

Characterization Method	Average Thickness (nm) for 42 layers of BPEI/PSS	Average Thickness (nm) for 42 layers of PDDA/PSS
Ellipsometry	354.0 ± 0.80	26.5 ± 0.18
AFM	342.8 ± 14.81	25.7 ± 2.68

Results obtained from AFM and ellipsometry are in good agreement. Note that ellipsometry is a reliable technique to determine thickness of thin films; however, ellipsometry may not provide reliable data at high thickness values. This is because of the depolarization of the light beam after reflections due to the light scattering from a rough surface [52].

4.1.2 Surface Morphology Analysis

AFM analysis was also conducted to determine surface morphology of multilayer films. AFM images of 42 layers of BPEI/PSS and PDDA/PSS films were illustrated in Figure 4.3. The surface roughness values (R_a) of BPEI/PSS and PDDA/PSS films were found as 38.8 nm and 12.5 nm, respectively.

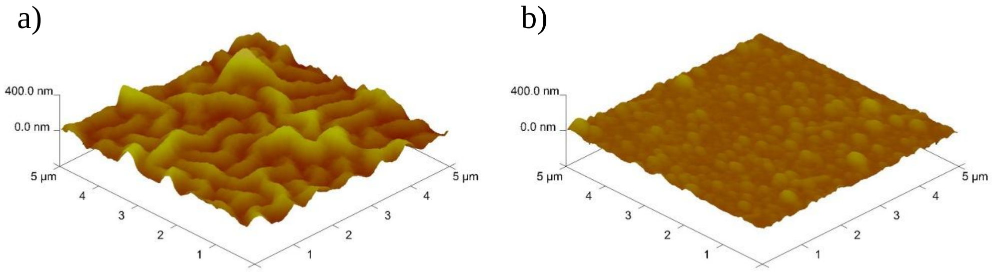

Figure 4.3 AFM height images of 42 layers of a) BPEI/PSS film b) PDDA/PSS film with 5 µm x 5 µm scan size.

As seen in Figure 4.3, the surface roughness of BPEI/PSS film is greater than that of PDDA/PSS film. This can be explained by the higher number of ionic crosslinks in PDDA/PSS films resulting in highly intense film structure. In contrast to PDDA/PSS films, BPEI/PSS had lower number of ionic crosslinks within the multilayers resulting in thicker and looser multilayers with greater surface roughness [49-51].

The difference between the surface morphologies of PDDA/PSS and BPEI/PSS films is also demonstrated for films with different number of layers (Figure 4.4). The roughness of BPEI/PSS film changes significantly from 2 to 61 layers. BPEI/PSS films have worm-like morphology which was reported for weak polyelectrolyte pairs, whereas PDDA/PSS films were found to have mountain-like morphology [53-55]. Table 4.3 shows average roughness (R_a) values of multilayer films with different number of layers.

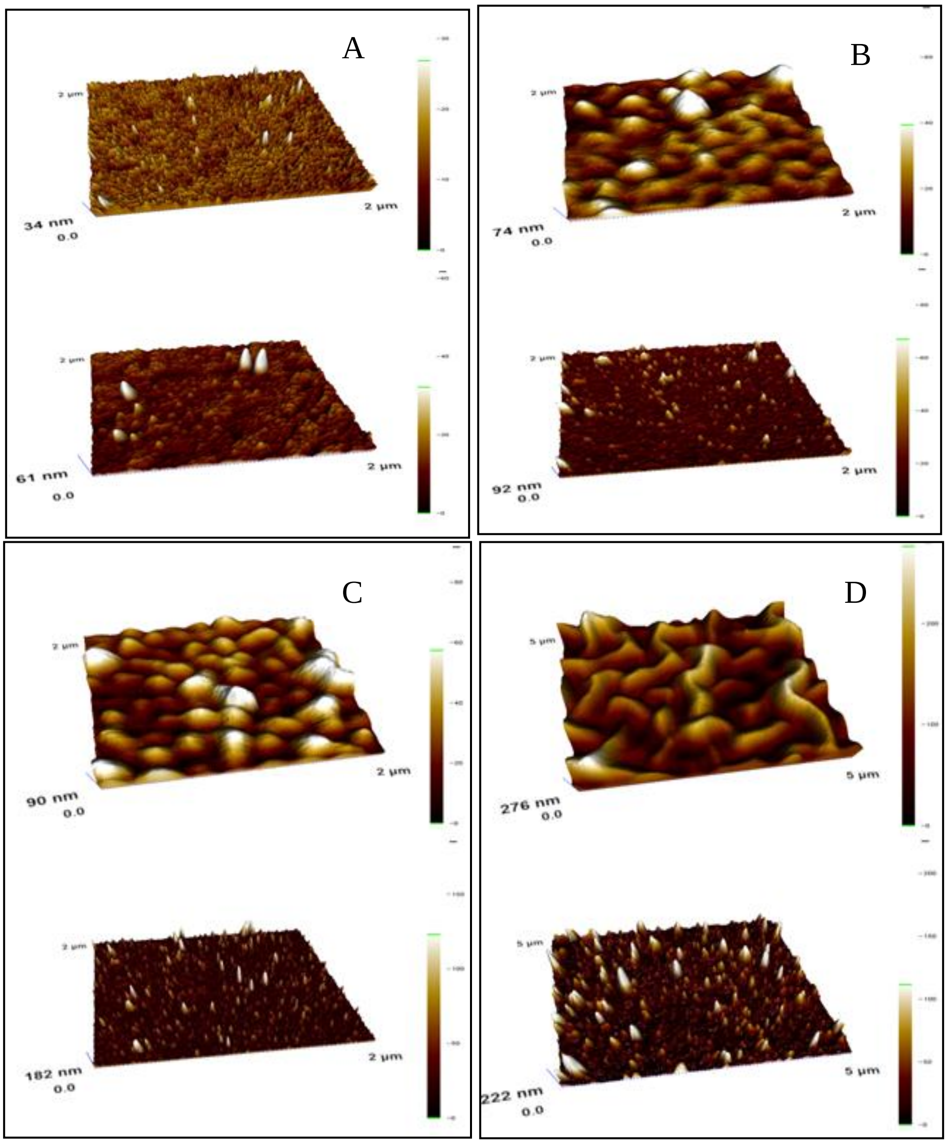

Figure 4.4 AFM images of BPEI/PSS (top) and PDDA/PSS (bottom) films; 2 layers (Panel A) with 2 µm x 2 µm scan size; 21 layers (Panel B) with 2 µm x 2 µm scan size; 41 layers (Panel C) with 2 µm x 2 µm scan size; 61 layers (Panel D) with 5 µm x 5 µm scan size.

Table 4.3 Average roughness (R_a) values of multilayer thin films.

Number of layers	R_a value of BPEI/PSS (nm)	R_a value of PDDA/PSS (nm)
2	1.78	2.45
21	8.69	4.50
41	10.32	8.05
61	38.92	13.84

4.2 Electrical Resistivity/Conductivity Measurements

Electrical resistivity/conductivity measurement experiments were conducted by two-point probe method. Volume resistivity changes were determined at different pressures. Figures 4.5 and 4.6 show logarithmic volume resistivity changes as a function of pressure for 2, 21, 41 and 61 layers of BPEI/PSS and PDDA/PSS films, respectively. When applied pressure is increased, logarithmic resistivity values decrease for 41 and 61 layers of BPEI/PSS and PDDA/PSS films. On the other hand, logarithmic resistivity values do not change with pressure for 2 and 21 layers of BPEI/PSS and PDDA/PSS. Volume resistivity and conductivity values of BPEI/PSS and PDDA/PSS films can be seen in Appendix B. Also, for comparison, resistivity values of ITO/glass were measured as a function of pressure and are illustrated in Figure 4.7. Resistance, volume resistivity and conductivity values of ITO/glass are demonstrated in Table 4.4.

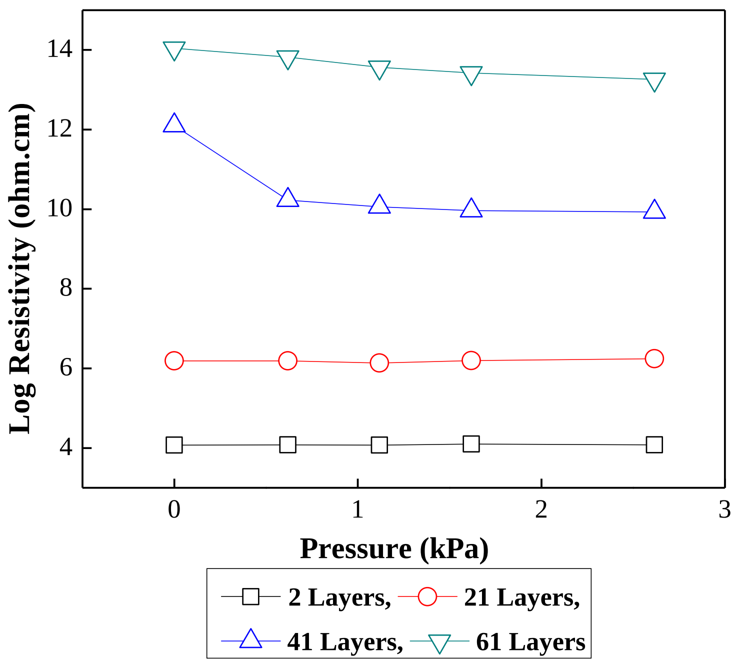

Figure 4.5 Logarithmic volume resistivity change as a function of pressure for BPEI/PSS films.

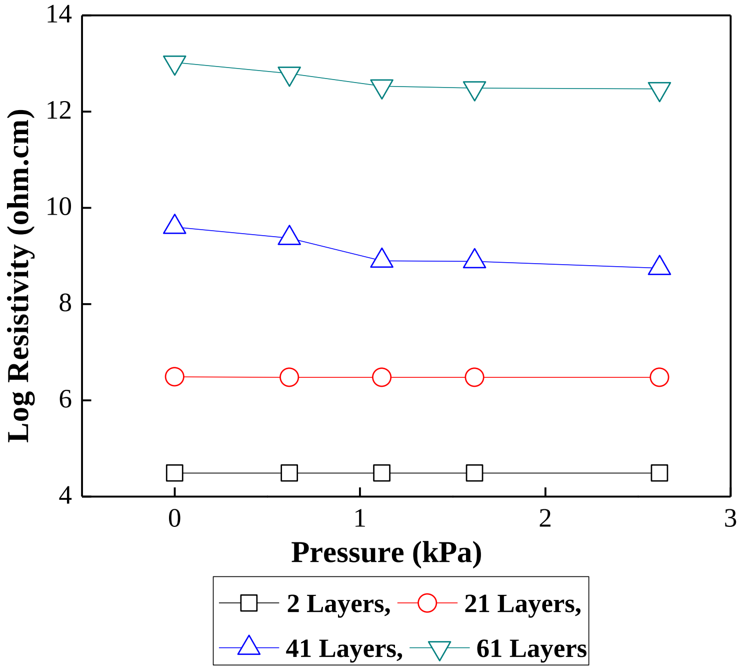

Figure 4.6 Logarithmic volume resistivity change as a function of pressure for PDDA/PSS films.

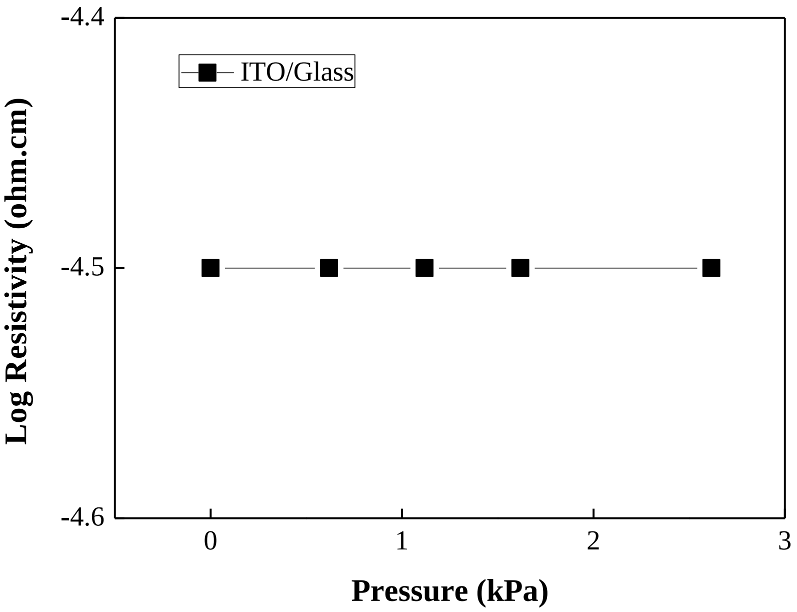

Figure 4.7 Logarithmic volume resistivity change as a function of pressure for ITO/glass.

As it is seen in the Figures 4.5 and 4.6, when applied pressure is increased, resistivity values of 41 and 61 layers of BPEI/PSS and PDDA/PSS films decrease and conductivity values increase. The increase in conductivity with increasing pressure may be correlated with the deformation of the film and re-orientation of the polymers within the multilayers leading to a change in charge carrier mechanism. A study by Qu and Wong stated that when pressure was applied to reinforced polymer material, resistivity decreases, and conductivity increases under compression. They explained this phenomenon by the formation of conductive paths within the material. They suggested that when applied pressure was increased, polymer was deformed and molecules within the material were re-oriented and if the molecules were aligned parallel to each other, large surface area was created for generation of electric fields. Hence, enhancement of electron hoping and charge carrier mechanisms were achieved [56].

The resistivity values of 2 and 21 layers of BPEI/PSS are slightly lower than resistivity values of 2 and 21 layers of PDDA/PSS. This difference can be correlated with the number of ionic crosslinks within the multilayers. As mentioned before, PDDA is a strong polyelectrolyte and the charge density on PDDA chains is greater than that on BPEI chains at pH 5. This would lead to higher amount of ionic crosslinks and lower number of free charge in PDDA/PSS films and lower conductivity. In addition, the extent of difference in the chain length between BPEI and PSS is higher than that between PDDA and PSS. Note that the number of repeating units for BPEI, PSS and PDDA was calculated as 50, 340 and 620-1200, respectively based on the molecular weights provided by the supplier company. A comparison of the chains lengths shows that the amount of negative free charge in BPEI/PSS multilayers is probably greater than the amount of free positive charges in PDDA/PSS multilayers, leading to higher conductivity of BPEI/PSS films.

Another consequence of the difference in the chain lengths could be the higher number of chain ends in BPEI/PSS films due to shorter BPEI chains resulting in higher amounts of voids within BPEI/PSS multilayers which might have affected the charge carrier mechanism in BPEI/PSS films.

To understand the effect of number of layers on the conductivity of the films, we have contrasted the logarithmic resistivity values for 2, 21, 41 and 61 layers. It was found that the change in logarithmic resistivity values was not significant for 2 and 21 layers films. The reason may be that the films were too thin to give any response when pressure was applied. Also, the lowest conductivity values were obtained for 61 layers due to higher amount of polymer material deposited at the surface, suppressing the conductivity of ITO/glass surface. The decrease in conductivity values with respect to number of layers was nine and ten order of magnitude for PDDA/PSS and BPEI/PSS films, respectively.

Resistance, volume resistivity and conductivity values of ITO/glass can be found in Table 4.4.

Table 4.4 ITO/Glass resistance, volume resistivity and conductivity values.

Pressure (kPa)	Average R (Ω)	Average ρ_v (Ω.cm)	Average δ (S/cm)
0	16.8 (±) 0.04	3.14×10^{-5} (±) 7.1×10^{-8}	3.2×10^{4}
0.62	16.8 (±) 0.71	3.14×10^{-5} (±) 1.4×10^{-6}	3.2×10^{4}
1.12	16.8 (±) 0.68	3.14×10^{-5} (±) 1.3×10^{-6}	3.2×10^{4}
1.62	16.9 (±) 0.75	3.16×10^{-5} (±) 1.4×10^{-6}	3.2×10^{4}
2.62	17.0 (±) 0.14	3.19×10^{-5} (±) 2.5×10^{-6}	3.1×10^{4}

Surface resistivity value of ITO/glass was given as 15-25 Ω/sq [46]. Using Equation 2 and resistance values that were obtained by two-point probe method, R_s value of ITO/glass was calculated as 24.4 Ω/sq. Therefore, similar surface resistivity value to the manufacturer data was obtained by two-point probe method. Resistance, volume resistivity and conductivity values of ITO/glass do not vary when pressure is applied. Additionally, conductivity value of ITO/glass (10^4 S/cm) is much higher than conductivity values of LbL films (~10^{-15} to ~10^{-5} S/cm). When volume resistivity and conductivity values of 2 layer films and ITO/glass are compared, the difference is almost nine order of magnitude. Although, there are only 2 layer on the ITO/glass substrate, difference of volume resistivity and conductivity values is significant.

4.3 Voltage Output Measurement

In order to understand piezoelectric property of LbL synthesized films, voltage output measurement was conducted. Pressure was applied to LbL films and voltage output was recorded. Voltage output of BPEI/PSS and PDDA/PSS films as a function of pressure can be seen in Figures 4.8 and 4.9, respectively. Raw data can be found in Appendix C. Additionally, crocodile clamps were hooked to the LbL films and ITO/glass, and voltage values resulting from the crocodiles were recorded in order to see their effect on the voltage output values. The voltage values at 0.62 and 2.62 kPa pressures are also given for comparison purposes and to see progress of voltage changes for the films. Results are presented in Tables 4.5 and 4.6.

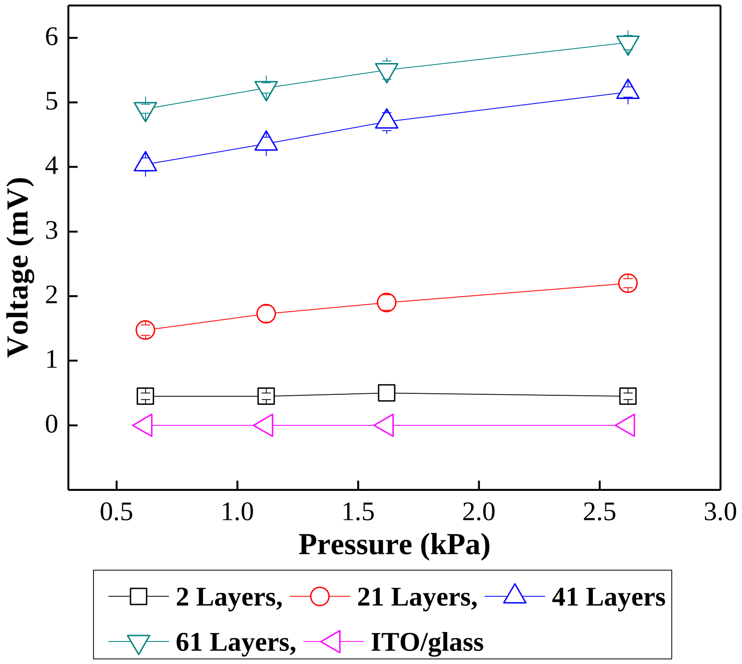

Figure 4.8 Voltage output as a function of pressure for BPEI/PSS films and ITO/glass.

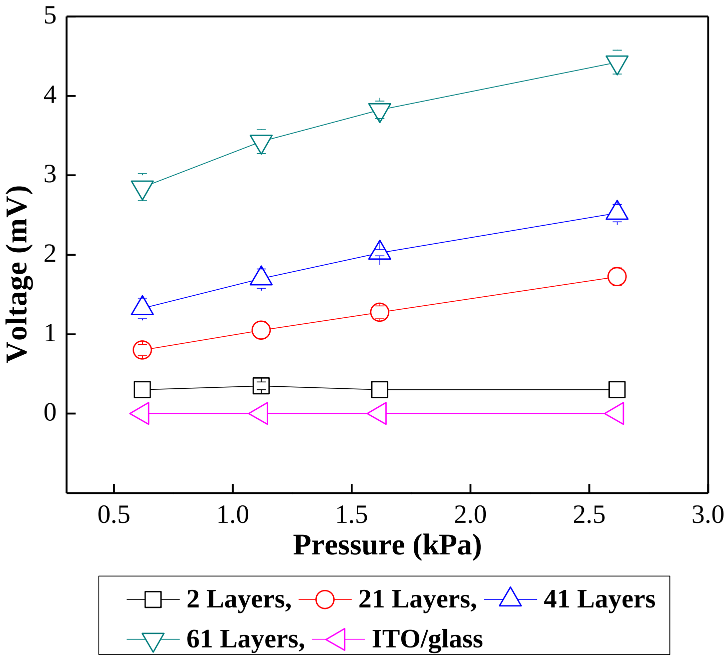

Figure 4.9 Voltage output as a function of pressure for PDDA/PSS films and ITO/glass.

Table 4.5 Voltage output values of BPEI/PSS with crocodile application only, and at 0.62 kPa and 2.62 kPa pressures.

Number of Layers	Voltage output (mV) with crocodile clamps only	Voltage output (mV) at 0.62 kPa	Voltage output (mV) at 2.62 kPa
2	0.5 (±) 0.05	0.5 (±) 0.05	0.5 (±) 0.05
21	0.7 (±) 0.04	1.5 (±) 0.08	2.2 (±) 0.07
41	2.0 (±) 0.08	4.0 (±) 0.10	5.2 (±) 0.08
61	2.4 (±) 0.07	4.9 (±) 0.07	5.9 (±) 0.11

Table 4.6 Voltage output values of PDDA/PSS with crocodile application only, and at 0.62 kPa and 2.62 kPa pressures.

Number of Layers	Voltage output (mV) with crocodile clamps only	Voltage output (mV) at 0.62 kPa	Voltage output (mV) at 2.62 kPa
2	0.3 (±) 0.05	0.3 (±) 0	0.3 (±) 0
21	0.5 (±) 0.05	0.8 (±) 0.07	1.7 (±) 0.11
41	0.6 (±) 0.04	1.3 (±) 0.13	2.5 (±) 0.11
61	1.0 (±) 0.11	2.9 (±) 0.17	4.4 (±) 0.15

Figures 4.8 and 4.9 demonstrate that the voltage increases linearly as the pressure is increased for 21, 41, 61 layers of BPEI/PSS and PDDA/PSS films. R^2 values of 21, 41 and 61 layers of BPEI/PSS films were found as 0.988, 0.992 and 0.985, respectively. Moreover, R^2 values of 21, 41 and 61 layers of PDDA/PSS films were found as 0.999, 0.970 and 0.954, respectively. R^2 values of 2 layers films could not be obtained because the voltages did not change with application of pressure. 61 layers of BPEI/PSS and PDDA/PSS generated 5.9 mV and 4.4 mV at 2.62 kPa, respectively. 2 layers of BPEI/PSS and PDDA/PSS did not give any response when pressure was applied. The reason may be that the films were too thin and were not appropriate for this type of experiment. A study by Zeng and coworkers [28] claimed that the film which was synthesized by ESA process showed piezoelectric property because of the approximately linear relationship between the voltage and applied force. Therefore, it can be said that LbL films may show piezoelectric property due to increase in voltage with increasing pressure. Note that, as expected voltage value of ITO/glass did not change with pressure application.

4.4 Displacement-Electric Field Hysteresis Loop

Displacement-electric field hysteresis loop analysis was performed by AFM to determine piezoelectric properties of the LbL films. Figure 4.10 demonstrates displacement changes with respect to electric field for 1, 2, 3, 21, 41 and 61 layers of PDDA/PSS films at 20 V and ITO/glass. Hysteresis amount (%), maximum strain (%) and d_{33} values of PDDA/PSS films at 20 V are tabulated in Table 4.7. Calculations of hysteresis amount (%), maximum strain (%) and d_{33} values for 21 layers of PDDA/PSS film can be found in Appendix D as an example.

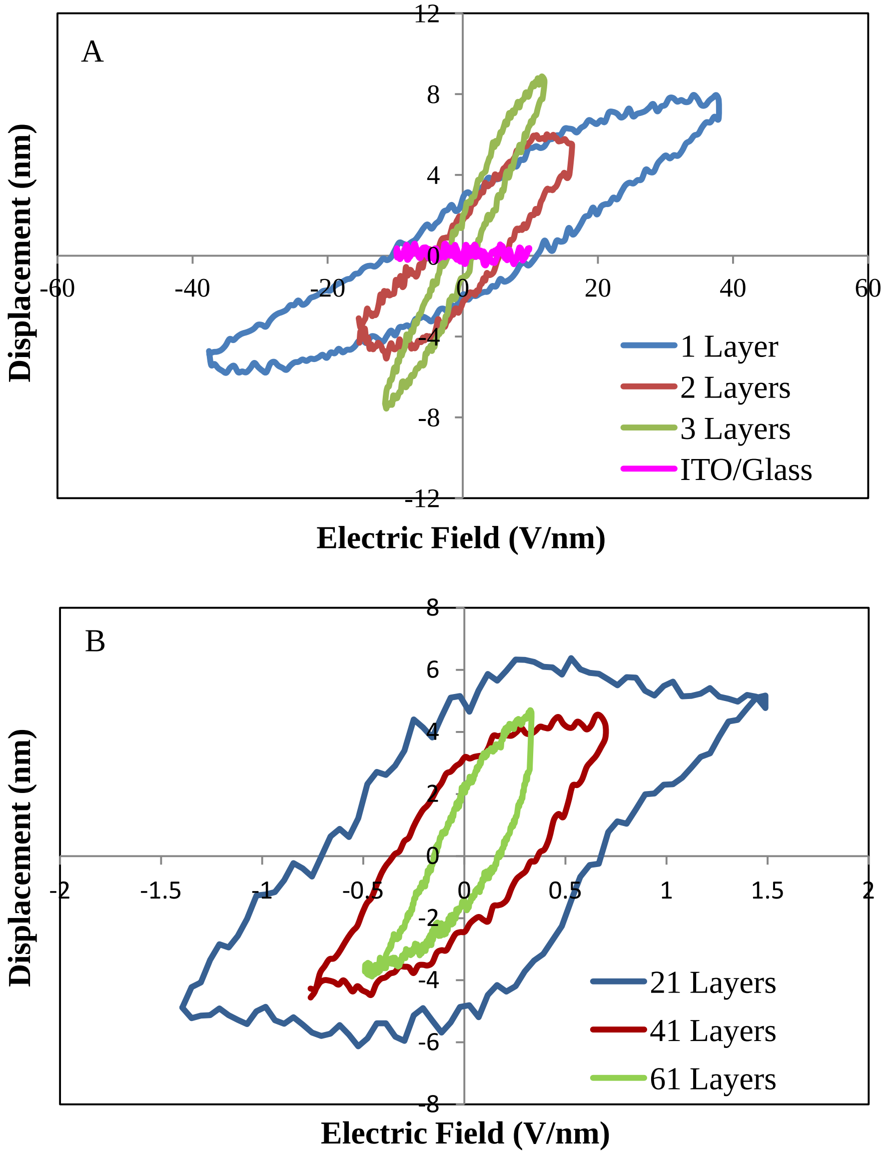

Figure 4.10 Displacement change with respect to electric field for PDDA/PSS films at 20 V; 1, 2, 3 layers and ITO/glass (Panel A); 21, 41 and 61 layers (Panel B).

Table 4.7 Hysteresis amount (%), maximum strain (%) and d_{33} values of 1, 2, 3, 21, 41 and 61 layers of PDDA/PSS films at 20 V.

Layer Number	Hysteresis Amount (%)	Maximum Strain (%)	d_{33} (Å/V)
1	40.3	2750	4.8
2	42.3	1482	4.8
3	21.1	1023	4.7
21	84.5	94.3	4.7
41	60.4	34.8	4.1
61	44.5	18.5	2.9

Symmetrical hysteresis loop is a typical ideal behavior of piezoelectric materials for which positive and negative coercive fields and remnant polarizations are equal [57]. The shape of the loop may change depending on the film thickness, preparation conditions, existence of impurities, charged defects, etc. The hysteretic behavior of LbL films can be seen in Figure 4.10. First, it can be said that all of the LbL films show piezoelectric behavior. As mentioned above, there are many factors which may affect the shape of the hysteresis loop of the films here. The displacement versus electric field relationship is complicated due to the competing effects of number of polyelectrolyte layers, their ionic crosslinking, their polarizability, number of free charges, etc. Therefore, it is not possible to relate all these factors with one another. Table 4.7 shows that when layer number is increased from 21 to 61, amount of hysteresis (%), maximum strain (%) and d_{33} values decrease. The increase in maximum strain values with decreasing number of layers is due to lower resistance of the thinner films according to the applied electric field. When 1, 2 and 3 layers are compared, it can be concluded that hysteresis amount (%) values of 1 and 2 layers are almost equal and they are higher than that of 3 layers. Furthermore, d_{33} values of 1, 2 and 3 layers are approximately the same because films were too thin. On the other hand, maximum strain values of 1, 2 and 3 layers seem somewhat suspicious due to their very high values compared to those of 21 or higher layers of the films. Further studies will be conducted to understand the unexpected high values of the maximum strain values for 1, 2 and 3 layer films.

Displacement change with respect to electric field for 1, 2 and 3 layers of BPEI/PSS films at 20 V and ITO/glass are represented in Figure 4.11. Displacement-electric field hysteresis loops of 21, 41 and 61 layers of BPEI/PSS films at 30 V are demonstrated in Figure 4.12 since Amount of hysteresis (%), maximum strain (%) and d_{33} values of 1, 2 and 3 layers of BPEI/PSS films at 20 V can be seen in Table 4.8. Table 4.9 shows amount of hysteresis (%), maximum strain (%) and d_{33} values of 21, 41 and 61 layers of BPEI/PSS films at 30 V.

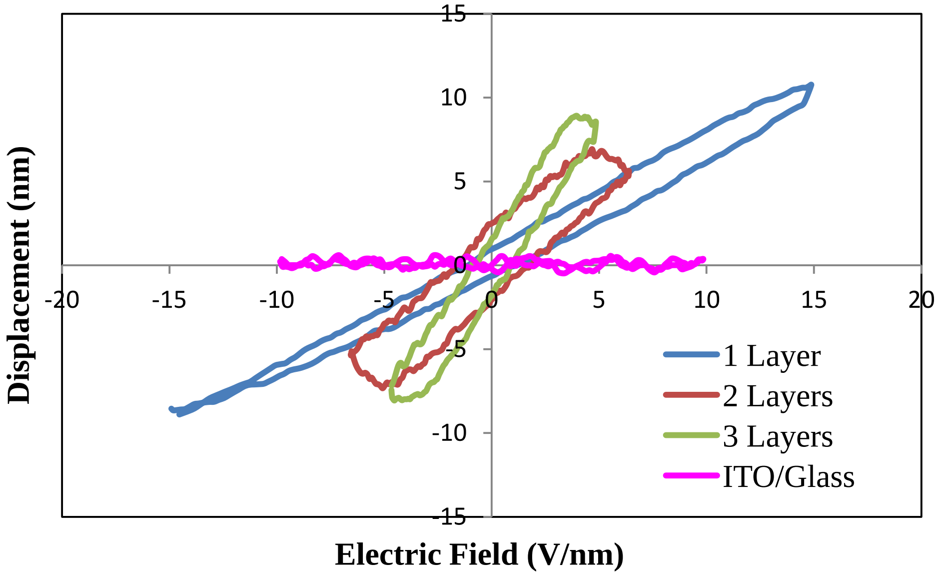

Figure 4.11 Displacement change with respect to electric field for 1, 2 and 3 layers of BPEI/PSS films at 20 V and ITO/glass.

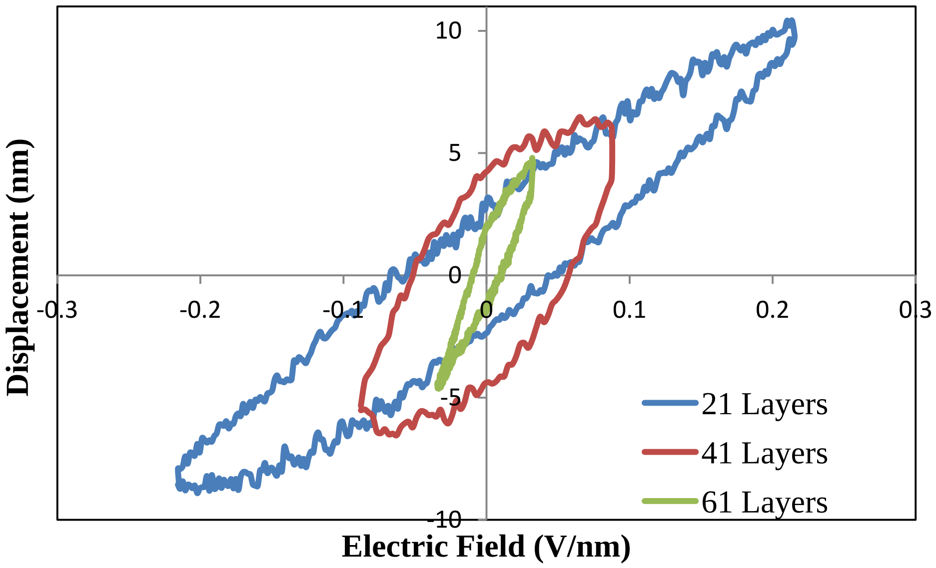

Figure 4.12 Displacement change with respect to electric field for 21, 41 and 61 layers of BPEI/PSS films at 30 V.

Table 4.8 Amount of hysteresis (%), maximum strain (%) and d_{33} values of BPEI/PSS films at 20 V.

Number of Layers	Hysteresis Amount (%)	Maximum Strain (%)	d_{33} (Å/V)
1	11.2	878	5.4
2	40.5	496	5.0
3	19.0	427	4.8

Table 4.9 Amount of hysteresis (%), maximum strain (%) and d_{33} values of BPEI/PSS films at 30 V.

Number of Layers	Hysteresis Amount (%)	Maximum Strain (%)	d_{33} (Å/V)
21	28.4	14.6	4.2
41	66.8	4.0	3.3
61	34.7	1.1	1.3

As it is seen in Table 4.9 and Figure 4.12, hysteresis amount (%) of 41 layers of BPEI/PSS is the highest, and followed by 61 and 21 layers of BPEI/PSS films. The reason may be attributed to the aforementioned factors. Additional film preparations may be needed for supporting the consistency of the results. Additionally, maximum strain (%) and d_{33} values decrease with increasing number of layers for all films. As electric field is applied, the response obtained would be lower as the multilayer structure gets thicker but looser with increasing number of layers. Thus, the maximum strain (%) value for 61 layer BPEI/PSS film was the lowest.

Figure 4.13 and Table 4.10 are given in order to compare two different multilayer films. Figure 4.13 illustrates displacement-electric field hysteresis loops of 1, 2, 3, 21 and 41 layers of BPEI/PSS and PDDA/PSS films at 20 V, and amount of hysteresis (%), maximum strain (%) and d_{33} values are tabulated in Table 4.10.

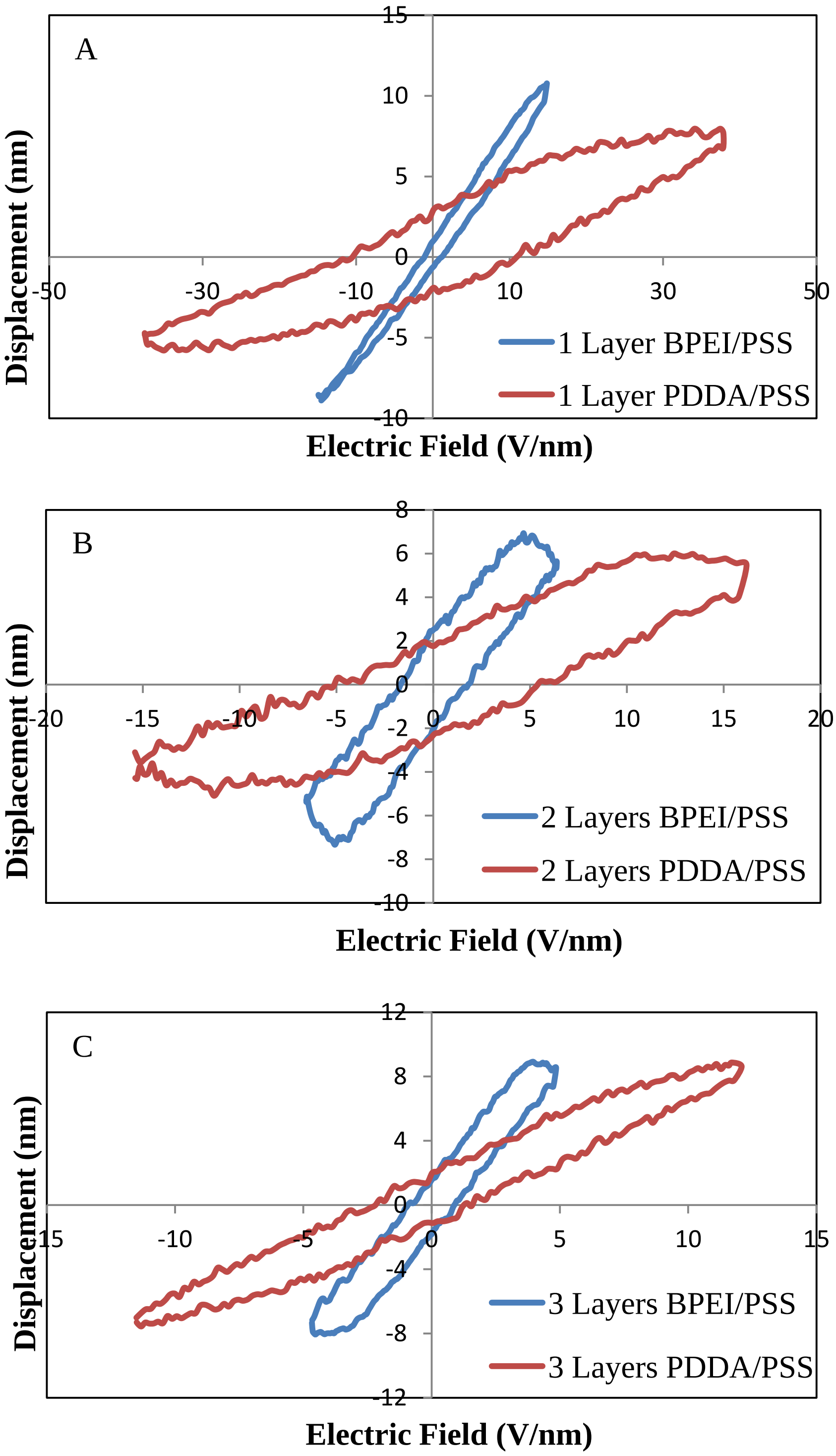

Figure 4.13 Displacement-electric field hysteresis loops of BPEI/PSS and PDDA/PSS films at 20 V; 1 layer (Panel A); 2 layers (Panel B); 3 layers (Panel C); 21 layers (Panel D); 41 layers (Panel E).

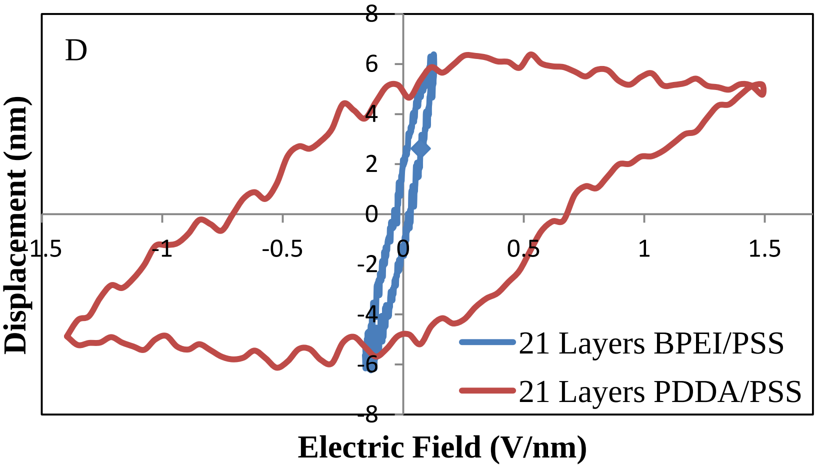

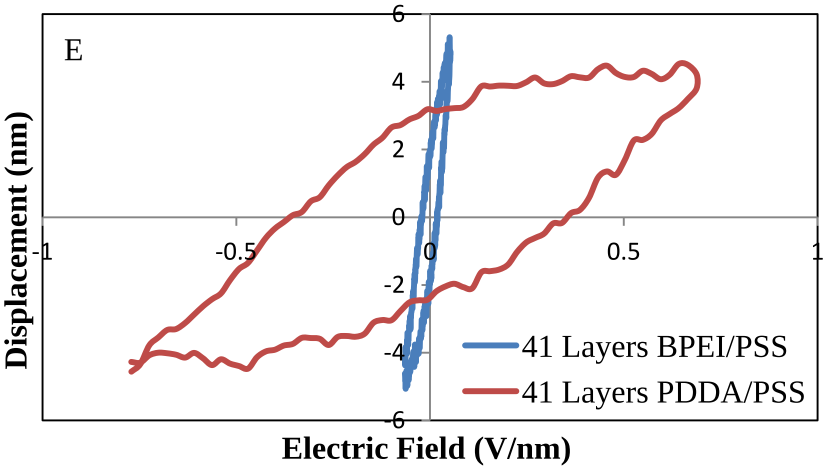

Figure 4.13 (Continued).

Table 4.10 Hysteresis amount (%), maximum strain (%) and d_{33} values of BPEI/PSS and PDDA/PSS films at 20 V.

Layer Number	Hysteresis Amount (%)		Maximum Strain (%)		d_{33} (Å/V)	
	BPEI/ PSS	PDDA/ PSS	BPEI/ PSS	PDDA/ PSS	BPEI/ PSS	PDDA/ PSS
1	11.2	40.3	878	2750	5.4	4.8
2	40.5	42.3	496	1482	5.0	4.8
3	19.0	21.1	427	1023	4.8	4.7
21	24.2	84.5	9.5	94.3	3.6	4.7
41	35.6	60.4	3.2	34.8	2.9	4.1
61	-	44.5	-	18.5	-	2.9

Hysteretic behavior of the films can be seen in Figure 4.13. Hysteresis amount (%) and maximum strain (%) values of BPEI/PSS films are lower than those of PDDA/PSS films. The material is called as soft material when coercive field (at zero displacement) is low and hysteresis loop is narrow. Additionally, if coercive field is high and hysteresis loop has large area, then the material is called as hard material [58]. Thus, when this statement is taken into consideration BPEI/PSS films are softer than PDDA/PSS films. It is reasonable because BPEI/PSS films have lower number ionic crosslinks than PDDA/PSS films resulting in thicker but looser structure [34]. Moreover, one characteristic property in piezoelectric materials is more dominant than the other one, in other words, direct piezoelectric effect which is conversion of mechanical energy to electrical energy can be dominant when it is compared with converse effect which is conversion of electrical energy to mechanical energy. Voltage output of 21 and 41 layers of BPEI/PSS films is greater than that of 21 and 41 layers of PDDA/PSS films. These results support that converse piezoelectricity of PDDA/PSS films are more dominant than that of BPEI/PSS films. Thus, it is reasonable to expect that hysteresis amount of PDDA/PSS film should be higher than BPEI/PSS film [59].

CHAPTER 5

CONCLUSIONS

Piezoelectric properties of two different polyelectrolyte multilayer films have been examined. Multilayers were prepared using layer-by-layer technique. The first multilayer system was composed of BPEI, a positively charged weak polyelectrolyte and PSS, a negatively charged strong polyelectrolyte. The second multilayer system was composed of PDDA, a positively charged strong polyelectrolyte and PSS.

In the first part, the conditions for successful LbL growth of BPEI/PSS and PDDA/PSS multilayers were optimized. The LbL growth profile for BPEI/PSS was found to be exponential at pH 5, whereas the thickness of PDDA/PSS films increased linearly as the number of layers increased. The difference in the growth profiles can be correlated with the number of ionic cross-links within the multilayers as well as the surface roughness. BPEI has lower charge density than that of PDDA, thus the number of ionic crosslinks is lower in BPEI/PSS multilayers, resulting in loopy film structure with greater surface roughness leading to an exponential film growth. PDDA/PSS films were smoother with lower surface roughness due to highly ionic cross-linked structure of the multilayers.

Furthermore, electrical resistivity/conductivity measurements were conducted to determine the electrical properties of the films. Resistivity values of 41 and 61 layer BPEI/PSS and PDDA/PSS films decreased (increase in conductivity) when the applied pressure was increased, whereas no change in resistivity was recorded for 2 and 21 layer BPEI/PSS and PDDA/PSS films.

In the second part, piezoelectric characterizations were performed. It was found that voltage-output values increased with increasing applied pressure as well as increasing number of layers for both BPEI/PSS and PDDA/PSS films. Increase in voltage output with increasing pressure suggested that LbL films may have piezoelectric characteristic.

In the last part, hysteresis loop analysis has been performed. Hysteresis loop is a characteristic of the piezoelectric materials. All LbL films showed hysteretic behavior, including the films with 1, 2 and 3 layers. Amount of hysteresis (%) and maximum strain (%) values of PDDA/PSS films at 20 V decreased with increasing number of layers. This can be explained by the decrease in conductivity when the number of layer is increased. Interestingly, the amount of hysteresis (%) and maximum strain (%) values of PDDA/PSS films were higher than those of BPEI/PSS films with the same number of layers. This may be due to highly ionic crosslinked structure of PDDA/PSS multilayers. d_{33} (piezoelectric coefficient) values of the films decreased when number of layer was increased from 21 to 61 layers.

REFERENCES

[1] Defaÿ, E. (Ed.). (2013). Integration of Ferroelectric and Piezoelectric Thin Films: Concepts and Applications for Microsystems. John Wiley and Sons.

[2] Dielectric. (2014). In Encyclopædia Britannica. Retrieved from http://global.britannica.com/EBchecked/topic/162630/dielectric (Accessed: 21-Apr-2015)

[3] Nelson, W. G. (2010). Piezoelectric materials: structure, properties, and applications / Wesley G. Nelson, editor. New York: Nova Science Publishers, c2010.

[4] Kawai, H. (1969). The Piezoelectricity of Poly(vinylidene fluoride), Japanese Journal of Applied Physics, 8, 975-976.

[5] Hsu, T. R. (2008). MEMS and Microsystems: Design, Manufacture, and Nanoscale Engineering. John Wiley and Sons.

[6] Hodges, P., Y. (2001). Electro-optical Properties of Ultra Thin Organic films. Master’s Thesis, University of Virginia Tech, Blacksburg, Virginia.

[7] Cooper, K. L. (1999). Electrostatic self-assembly of linear and nonlinear optical thin films (Doctoral dissertation, Virginia Polytechnic Institute and State University).

[8] Kim, J., Loh, K. J., and Lynch, J. P. (2008). Piezoelectric Polymeric Thin Films Tuned By Carbon Nanotube Fillers, In The 15th International Symposium on: Smart Structures and Materials and Nondestructive Evaluation

and Health Monitoring (693232), International Society for Optics and Photonics.

[9] Rao, S. S., and Sunar, M. (1994). Piezoelectricity and its use in disturbance sensing and control of flexible structures: a survey, Applied Mechanics Reviews, 47(4), 113-123.

[10] Vatansever, D., Siores, E., and Shah, T. (2012). Alternative Resources for Renewable Energy: Piezoelectric and Photovoltaic Smart Structures, Global Warming–Impacts and Future Perspective, 263.

[11] Ledoux, A. (2011). Theory of piezoelectric materials and their applications in civil engineering (Doctoral dissertation, Massachusetts Institute of Technology).

[12] Fukada, E. (1998) History and Recent Progress in Piezoelectric Polymer Research, Proc. of IEEE Ultrasonic Symposium, 597-605.

[13] Konka, H. P. (2010). Characterization of composite piezoelectric materials for smart joint applications (Doctoral dissertation, Faculty of the Louisiana State University and Agricultural and Mechanical College in partial fulfillment of the requirements for degree of Master of Science in Mechanical Engineering In The Department of Mechanical Engineering by Hari Prasad Konka B. Tech, Jawaharlal Nehru Technological University).

[14] Zeng, T., Claus, R. O., Liu, Y., Zhang, F., Wei, W., and Cooper, K. L. (2000). Synthesis of piezoelectric thin films by molecular self-assembly, InSPIE's 7th Annual International Symposium on Smart Structures and Materials (171-176), International Society for Optics and Photonics.

[15] Cardoso, V. F., Minas, G., and Lanceros-Méndez, S. (2012). Multilayer spin-coating deposition of poly (vinylidene fluoride) films for controlling thickness and piezoelectric response, Sensors and Actuators A: Physical, 192, 76-80.

[16] Sharma, T., Je, S. S., Gill, B., and Zhang, J. X. (2012). Patterning piezoelectric thin film PVDF–TrFE based pressure sensor for catheter application, Sensors and Actuators A: Physical, 177, 87-92.

[17] Mao, D., Gnade, B. E., and Quevedo-Lopez, M. A. (2011). Ferroelectric Properties and Polarization Switching Kinetic of Poly(Vinylidene Fluoride-Trifluoroethylene) Copolymer.

[18] Wang, D., Liu, J., Zhou, D., and Huang, S. (1999). Using PVDF piezoelectric film sensors for in situ measurement of stayed-cable tension of cable-stayed bridges, Smart Materials and Structures, 8(5), 554.

[19] Wang, D. H., and Huang, S. L. (2000). Health Monitoring and Diagnosis for Flexible Structures with PVDF Piezoelectric Film Sensor Array, Journal of Intelligent Material Systems and Structures, 11(6), 482-491.

[20] Bauer, F. (2000). PVDF shock sensors: Applications to polar materials and high explosives, Ultrasonics, Ferroelectrics and Frequency Control, IEEE Transactions on, 47(6), 1448-1454.

[21] Monkhouse, R. S. C., Wilcox, P. D., and Cawley, P. (1997). Flexible interdigital PVDF transducers for the generation of Lamb waves in structures, Ultrasonics, 35(7), 489-498.

[22] Wegener, M., Oehler, H., Lellinger, D., and Alig, I. (2012). Note: Piezoelectric polymers as transducers for the ultrasonic-reflection method and

the application in mechanical property-screening of coatings, Review of Scientific Instruments, 83(1), 016102.

[23] Sato, T., Ishida, H., and Ikeda, O. (1980). Adaptive PVDF piezoelectric deformable mirror system, Applied Optics, 19(9), 1430-1434.

[24] Wang, X. (2011). Piezoelectric nanogenerators-harvesting ambient mechanical energy at the nanometer scale, Nano Energy, 1(1), 13-24.

[25] Shenck, N. S., and Paradiso, J. A. (2001). Energy scavenging with shoe-mounted piezoelectrics, IEEE Micro, 21(3), 30-42.

[26] Granstrom, J., Feenstra, J., Sodano, H. A., and Farinholt, K. (2007). Energy harvesting from a backpack instrumented with piezoelectric shoulder straps, Smart Materials and Structures, 16(5), 1810.

[27] Lang, S. B., and Muensit, S. (2006). Review of some lesser-known applications of piezoelectric and pyroelectric polymers, Applied Physics A, 85(2), 125-134.

[28] Zeng, T., Claus, R., Liu, Y., Zhang, F., Du, W., and Cooper, K. L. (2000). Piezoelectric ultrathin polymer films synthesized by electrostatic self-assembly processing, Smart Materials and Structures, 9(6), 801.

[29] Zeng, T., Claus, R., Zhang, F., Du, W., and Cooper, K. L. (2001). Ultrathin film actuators fabricated by layer-by-layer molecular self-assembly, Smart Materials and Structures, 10(4), 780.

[30] Hammond, P. T. (1999). Recent explorations in electrostatic multilayer thin film assembly, Current Opinion in Colloid and Interface Science, 4(6), 430-442.

[31] Guanglu Wu and Xi Zhang (2010). Unconventional Layer-by-Layer Assembly for Functional Organic Thin Films, Polymer Thin Films, Abbass A Hashim (Ed.), ISBN: 978-953-307-059-9, InTech, DOI: 10.5772/8388. Available from: http://www.intechopen.com/books/polymer-thin-films/unconventional-layer-by-layer-assembly-for-functional-organic-thin-films (Accessed: 21-Apr-2015)

[32] Tsukruk, V. V. (1997). Assembly of supramolecular polymers in ultrathin films, Progress in Polymer Science, 22(2), 247-311.

[33] Schönhoff, M. (2003). Self-assembled polyelectrolyte multilayers, Current Opinion in Colloid and Interface Science, 8(1), 86-95.

[34] Lutkenhaus, J. L., and Hammond, P. T. (2007). Electrochemically enabled polyelectrolyte multilayer devices: from fuel cells to sensors, Soft Matter, 3(7), 804-816.

[35] Ashcraft, J. N., Argun, A. A., and Hammond, P. T. (2010). Structure-property studies of highly conductive layer-by-layer assembled membranes for fuel cell PEM applications, Journal of Materials Chemistry, 20(30), 6250-6257.

[36] Yu-Xiang Zheng, Rong-Jun Zhang and Liang-Yao Chen (2012). Ellipsometry and Its Applications in Stoichiometry, Stoichiometry and Materials Science - When Numbers Matter, Dr. Alessio Innocenti (Ed.), ISBN: 978-953-51-0512-1, InTech, Available from: http://www.intechopen.com/books/stoichiometry-and-materialsscience-when-numbers-matter/ellipsometry-and-its-application-in-stoichiometry (Accessed: 21-Apr-2015)

[37] Schiefelbein, S. L., Fried, N. A., Rhoads, K. G., and Sadoway, D. R. (1998). A high-accuracy, calibration-free technique for measuring the electrical conductivity of liquids, Review of Scientific Instruments, 69(9), 3308-3313.

[38] Enderling, S., Brown III, C. L., Smith, S., Dicks, M. H., Stevenson, J., Mitkova, M., and Walton, A. J. (2006). Sheet resistance measurement of non-standard cleanroom materials using suspended Greek cross test structures, Semiconductor Manufacturing, IEEE Transactions on, 19(1), 2-9.

[39] Surface resistivity. (2001). In Keithley. Retrieved from http://www.keithley.com/data?asset=6069 (Accessed: 21-Apr-2015)

[40] He, J., Zeng, R., and Zhang, B. (2012). Methodology and Technology for Power System Grounding. John Wiley and Sons.

[41] Li, J. C., Wang, Y., and Ba, D. C. (2012). Characterization of semiconductor surface conductivity by using microscopic four-point probe technique, Physics Procedia, 32, 347-355.

[42] Haugstad, G. (2012). Atomic force microscopy: understanding basic modes and advanced applications, John Wiley and Sons.

[43] Heimann, R. B. (2010). Classic and advanced ceramics: from fundamentals to applications, John Wiley and Sons.

[44] Lefki, K., and Dormans, G. J. M. (1994). Measurement of piezoelectric coefficients of ferroelectric thin films. Journal of applied physics, 76(3), 1764-1767.

[45] Claus, R. O., Zeng, T., and Liu, Y. (2002). U.S. Patent No. 6,447,887. Washington, DC: U.S. Patent and Trademark Office.

[46] Sigma-Aldrich Co. (2014). Retrieved from http://www.sigmaaldrich.com/catalog/product/aldrich/636916?lang=en&region=TR (Accessed: 21-Apr-2015)

[47] Gadelmawla, E. S., Koura, M. M., Maksoud, T. M. A., Elewa, I. M., and Soliman, H. H. (2002). Roughness parameters. Journal of Materials Processing Technology, 123(1), 133-145.

[48] Wang, Z., Hauser, P. J., Laine, J., and Rojas, O. J. (2011). Multilayers of low charge density polyelectrolytes on thin films of carboxymethylated and cationic cellulose, Journal of Adhesion Science and Technology, 25(6-7), 643-660.

[49] Tong, W., Gao, C., and Möhwald, H. (2006). Stable weak polyelectrolyte microcapsules with pH-responsive permeability, Macromolecules, 39(1), 335-340.

[50] de Saint-Aubin, C., Hemmerlé, J., Boulmedais, F., et al. (2012). New 2-in-1 polyelectrolyte step-by-step film buildup without solution alternation: from PEDOT-PSS to polyelectrolyte complexes, Langmuir, 28(23), 8681-8691.

[51] Shiratori, S. S., and Rubner, M. F. (2000). pH-dependent thickness behavior of sequentially adsorbed layers of weak polyelectrolytes. Macromolecules, 33(11), 4213-4219.

[52] Carlin, C. M., Kepley, L. J., & Bard, A. J. (1985). Polymer Films on Electrodes XVI. In Situ Ellipsometric Measurements of Polybipyrazine, Polyaniline, and Polyvinylferrocene Films. Journal of the Electrochemical Society, 132(2), 353-359.

[53] McAloney, R. A., Sinyor, M., Dudnik, V., and Goh, M. C. (2001). Atomic force microscopy studies of salt effects on polyelectrolyte multilayer film morphology, Langmuir, 17(21), 6655-6663.

[54] Espinosa-González, C., Moggio, I., Arias-Marın, E., Romero-Garcıa, J., Cruz-Silva, R., Le Moigne, J., and Ortiz-Cisneros, J. (2003). Layer-by-layer assembled films of a rigid poly (phenyl-ethynylene) and alternate poly (phenyl-ethynylene)/poly (aniline), Synthetic Metals, 139(1), 155-161.

[55] Baowei, S. U., Wang, T., Wang, Z., Gao, X., and Gao, C. (2012). Preparation and performance of dynamic layer-by-layer PDADMAC/PSS nanofiltration membrane, Journal of Membrane Science, 423, 324-331.

[56] Qu, S., and Wong, S. C. (2007). Piezoresistive behavior of polymer reinforced by expanded graphite, Composites Science and Technology, 67(2), 231-237.

[57] Damjanovic, D. (2006). Hysteresis in piezoelectric and ferroelectric materials, The Science of Hysteresis, 3, 337-465.

[58] Mehta, V.K., and Mehta R. (2006). Basic Electrical Engineering (4th ed.), S. Chand and Company Ltd., New Delhi.

[59] Chen, Q. X., and Payne, P. A. (1995). Industrial applications of piezoelectric polymer transducers, Measurement Science and Technology, 6(3), 249.

APPENDIX A

AFM ANALYSIS

Table A.1 Thickness results of AFM analysis for 42 layers of BPEI/PSS and PDDA/PSS films.

Measurement Number	Thickness (nm) for 42 Layers of BPEI/PSS	Thickness (nm) for 42 Layers of PDDA/PSS
1	322.5	25.7
2	357.3	22.2
3	342.5	23.3
4	341.0	26.0
5	393.0	29.7
6	330.8	26.4
7	322.1	30.1
8	330.1	27.4
9	359.9	23.7
10	328.3	22.5
Mean	342.8	25.7
Standard Deviation (±)	14.8	2.7

APPENDIX B

ELECTRICAL RESISTIVITY/CONDUCTIVITY MEASUREMENT

Table B.1 Electrical resistivity and conductivity values of 2 Layers of BPEI/PSS film.

Pressure (kPa)	Average ρ_v (Ω.cm)	Standard Deviation of ρ_v (±)	Average δ (S/cm)
0	1.18×10^{4}	3.6×10^{2}	8.5×10^{-5}
0.62	1.19×10^{4}	9.5×10^{2}	8.4×10^{-5}
1.12	1.18×10^{4}	1.0×10^{3}	8.5×10^{-5}
1.62	1.25×10^{4}	7.5×10^{2}	8.0×10^{-5}
2.62	1.20×10^{4}	1.1×10^{3}	8.3×10^{-5}

Table B.2 Electrical resistivity and conductivity values of 21 Layers of BPEI/PSS film.

Pressure (kPa)	Average ρ_v (Ω.cm)	Standard Deviation of ρ_v (±)	Average δ (S/cm)
0	1.55×10^{6}	3.2×10^{5}	6.5×10^{-7}
0.62	1.56×10^{6}	5.2×10^{5}	6.4×10^{-7}
1.12	1.36×10^{6}	3.2×10^{5}	7.4×10^{-7}
1.62	1.57×10^{6}	4.6×10^{5}	6.3×10^{-7}
2.62	1.75×10^{6}	6.5×10^{5}	5.7×10^{-7}

Table B.3 Electrical resistivity and conductivity values of 41 Layers of BPEI/PSS film.

Pressure (kPa)	Average ρ_v (Ω.cm)	Standard Deviation of ρ_v (±)	Average δ (S/cm)
0	1.26×10^{12}	2.2×10^{11}	7.9×10^{-13}
0.62	1.68×10^{10}	4.3×10^{9}	6.0×10^{-11}
1.12	1.15×10^{10}	1.5×10^{9}	8.7×10^{-11}
1.62	9.21×10^{9}	5.7×10^{8}	1.1×10^{-10}
2.62	8.47×10^{9}	4.2×10^{8}	1.2×10^{-11}

Table B.4 Electrical resistivity and conductivity values of 61 Layers of BPEI/PSS film.

Pressure (kPa)	Average ρ_v (Ω.cm)	Standard Deviation of ρ_v (±)	Average δ (S/cm)
0	1.09×10^{14}	1.3×10^{13}	9.2×10^{-15}
0.62	6.60×10^{13}	8.3×10^{12}	1.5×10^{-14}
1.12	3.67×10^{13}	3.9×10^{12}	2.7×10^{-14}
1.62	2.64×10^{13}	5.4×10^{12}	3.8×10^{-14}
2.62	1.82×10^{13}	4.9×10^{12}	5.5×10^{-14}

Table B.5 Electrical resistivity and conductivity values of 2 Layers of PDDA/PSS film.

Pressure (kPa)	Average ρ_v (Ω.cm)	Standard Deviation of ρ_v (±)	Average δ (S/cm)
0	3.10×10^{4}	3.0×10^{3}	3.2×10^{-5}
0.62	3.06×10^{4}	3.7×10^{2}	3.3×10^{-5}
1.12	3.11×10^{4}	7.3×10^{2}	3.2×10^{-5}
1.62	3.12×10^{4}	2.8×10^{2}	3.2×10^{-5}
2.62	3.09×10^{4}	9.6×10^{2}	3.2×10^{-5}

Table B.6 Electrical resistivity and conductivity values of 21 Layers of PDDA/PSS film.

Pressure (kPa)	Average ρ_v (Ω.cm)	Standard Deviation of ρ_v (±)	Average δ (S/cm)
0	3.09×10^{6}	4.2×10^{5}	3.2×10^{-7}
0.62	3.04×10^{6}	2.3×10^{5}	3.3×10^{-7}
1.12	3.00×10^{6}	1.1×10^{5}	3.3×10^{-7}
1.62	3.00×10^{6}	1.9×10^{5}	3.3×10^{-7}
2.62	2.99×10^{6}	2.2×10^{5}	3.3×10^{-7}

Table B.7 Electrical resistivity and conductivity values of 41 Layers of PDDA/PSS film.

Pressure (kPa)	Average ρ_v (Ω.cm)	Standard Deviation of ρ_v (±)	Average δ (S/cm)
0	3.98×10^{9}	2.6×10^{8}	2.5×10^{-10}
0.62	2.35×10^{9}	9.5×10^{7}	8.6×10^{-10}
1.12	7.95×10^{8}	6.0×10^{7}	1.3×10^{-9}
1.62	7.74×10^{8}	5.5×10^{7}	1.3×10^{-9}
2.62	5.64×10^{8}	3.2×10^{7}	1.8×10^{-9}

Table B.8 Electrical resistivity and conductivity values of 61 Layers of PDDA/PSS film.

Pressure (kPa)	Average ρ_v (Ω.cm)	Standard Deviation of ρ_v (±)	Average δ (S/cm)
0	1.05×10^{13}	2.1×10^{12}	9.5×10^{-14}
0.62	6.21×10^{12}	2.8×10^{10}	1.6×10^{-13}
1.12	3.36×10^{12}	3.7×10^{11}	3.0×10^{-13}
1.62	3.11×10^{12}	2.6×10^{11}	3.2×10^{-13}
2.62	2.96×10^{12}	3.0×10^{11}	3.4×10^{-13}

APPENDIX C

VOLTAGE OUTPUT MEASUREMENT

Table C.1 Voltage change for 2 Layers of BPEI/PSS film.

Pressure (kPa)	Average Voltage (mV)	Standard Deviation (±)
Crocodile Clamps	0.45	0.05
0.62	0.45	0.05
1.12	0.45	0.05
1.62	0.50	-
2.62	0.45	0.05

Table C.2 Voltage change for 21 Layers of BPEI/PSS film.

Pressure (kPa)	Average Voltage (mV)	Standard Deviation (±)
Crocodile Clamps	0.73	0.04
0.62	1.48	0.08
1.12	1.73	0.13
1.62	1.90	0.12
2.62	2.20	0.07

Table C.3 Voltage change for 41 Layers of BPEI/PSS film.

Pressure (kPa)	Average Voltage (mV)	Standard Deviation (±)
Crocodile Clamps	2.02	0.08
0.62	4.04	0.10
1.12	4.36	0.10
1.62	4.70	0.14
2.62	5.16	0.08

Table C.4 Voltage change for 61 Layers of BPEI/PSS film.

Pressure (kPa)	Average Voltage (mV)	Standard Deviation (±)
Crocodile Clamps	2.4	0.07
0.62	4.9	0.07
1.12	5.2	0.08
1.62	5.5	0.14
2.62	5.9	0.11

Table C.5 Voltage change for 2 Layers of PDDA/PSS film.

Pressure (kPa)	Average Voltage (mV)	Standard Deviation (±)
Crocodile Clamps	0.3	0.05
0.62	0.3	-
1.12	0.4	0.05
1.62	0.3	-
2.62	0.3	-

Table C.6 Voltage change for 21 Layers of PDDA/PSS film.

Pressure (kPa)	Average Voltage (mV)	Standard Deviation (±)
Crocodile Clamps	0.45	0.05
0.62	0.80	0.07
1.12	1.05	0.11
1.62	1.28	0.08
2.62	1.73	0.11

Table C.7 Voltage change for 41 Layers of PDDA/PSS film.

Pressure (kPa)	Average Voltage (mV)	Standard Deviation (±)
Crocodile Clamps	0.63	0.04
0.62	1.33	0.13
1.12	1.70	0.12
1.62	2.03	0.04
2.62	2.53	0.11

Table C.8 Voltage change for 61 Layers of PDDA/PSS film.

Pressure (kPa)	Average Voltage (mV)	Standard Deviation (±)
Crocodile Clamps	0.95	0.11
0.62	2.85	0.17
1.12	3.43	0.15
1.62	3.83	0.11
2.62	4.43	0.15

APPENDIX D

HYSTERESIS LOOP ANALYSIS

Sample Calculations of Amount of Hysteresis (%), Maximum Strain (%) and d_{33} Values

The largest difference of displacement at any voltages is denoted as $D_{largest}$. D_T is the total displacement change and T_f is the thickness of film. Hysteresis amount (%), maximum strain (%) and d_{33} values of 21 layers of PDDA/PSS films at 20 V are calculated below. Figure D.1 illustrates determination of $D_{largest}$ and D_T values of 21 layers of PDDA/PSS film. Displacement and voltage changes of linear portion of hysteresis loop are represented as ΔD and ΔV, respectively. Figure D.2 is the illustration of determination of d_{33} value of 21 layer PDDA/PSS film.

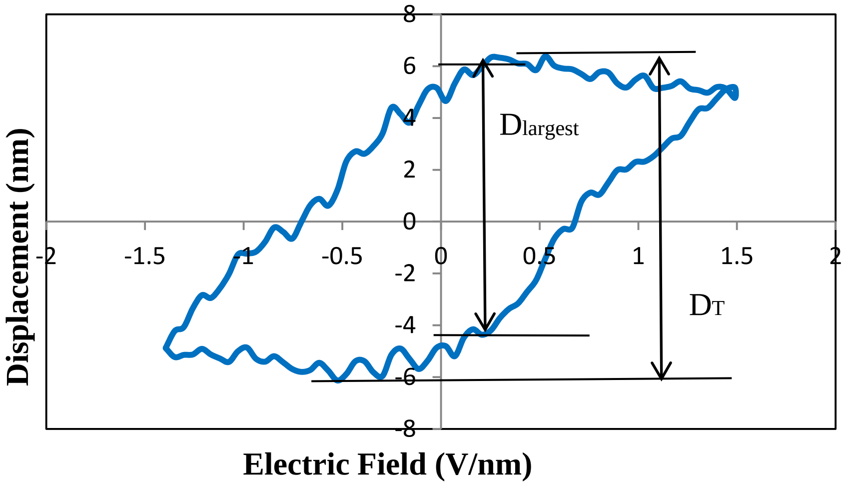

Figure D.1 Illustration of determination of $D_{largest}$ and D_T values of 21 layer PDDA/PSS film.

Calculations of hysteresis amount (%) and maximum strain (%) values of 21 layers of PDDA/PSS at 20 V can be seen in Equations D.1 and D.2, respectively.

$$\text{Hysteresis amount (\%)} = (D_{largest}/\ D_T) \times 100 \qquad \text{(D.1)}$$
$$= (10.53/12.46) \times 100$$
$$= 84.46\ \%$$

$$\text{Maximum strain (\%)} = (D_T/T_f) \times 100 \qquad \text{(D.2)}$$
$$= (12.46/13.22) \times 100$$
$$= 94.30\ \%$$

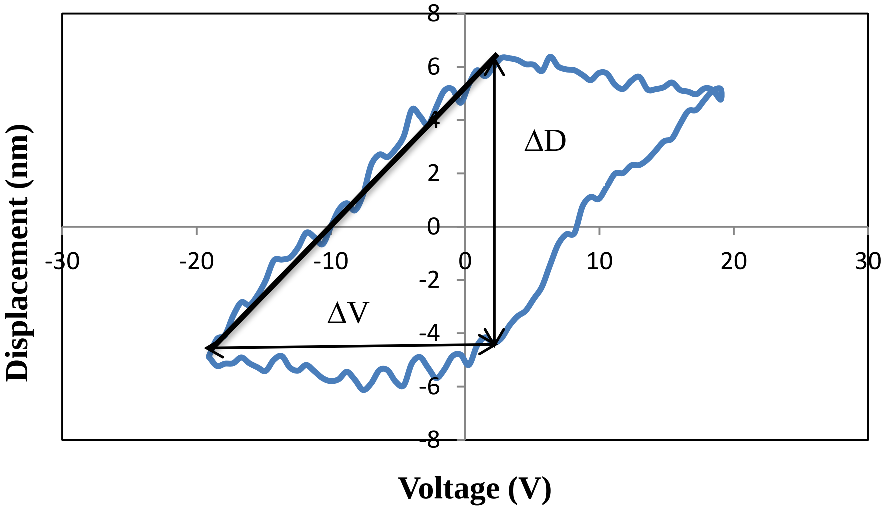

Figure D.2 Illustration of determination of d_{33} value of 21 layer PDDA/PSS film.

Calculation of d_{33} value of 21 layers of PDDA/PSS at 20 V can be seen in Equation D.3.

$$d_{33} = \Delta D/\Delta V \qquad \text{(D.3)}$$
$$= (10.3\ \text{nm})/(21.8\ \text{V})$$
$$d_{33} = 0.47\ \text{nm/V} = 4.7\ \text{Å/V}$$